



**Politecnico  
di Torino**

**Politecnico di Torino**

Master's Degree in Energy and Nuclear Engineering  
A.y. 2021/2022  
July 2022

# **Advanced multiple principal element alloys as structural material in ARC: neutronic and activation analysis**

Supervisors :

prof. Massimo Zucchetti  
prof.ssa Raffaella Testoni

Candidate:

Federico Ledda

Co-Supervisors:

dr. Stefano Segantin  
dr. Samuele Meschini



## Abstract

While the problem of global warming is becoming increasingly urgent, the geopolitical situation is underlining the necessity of include in the Italian energetic mix sources other than oil and gas. Conversely, the public opinion is still frightened by fission technologies, forcing governments to invest in different solutions. Great efforts have been spent in nuclear fusion research and the availability of new technologies in these years (e.g., high temperature superconductive magnets) are making it appear as a credible medium-term solution. The ARC project, proposed by scientist of the MIT and PSFC is aiming to prove the feasibility of such a technology, with a grid connected reactor. The present Thesis, developed in collaboration with M.I.T., investigates new structural materials for TBR enhancement in ARC (high entropy alloys) and activation studies. After the construction of a D-like model for a poloidal section of the torus, neutronic studies were conducted, using a classical Montecarlo approach; OpenMC, a tool developed at MIT, has been used for this purpose. The results are strongly encouraging, proving in theory the possibility of eliminating the Be layer from the layout thanks to the usage of innovative materials; a study on the impact of each element on the alloys performances have been conducted, to steer further investigations. The activation analysis that followed, conducted with the tool FISPACT-II, confirmed the superiority of high entropy alloys also in this regard, allowing a faster decay for irradiated material and the possibility of recycling in a time scale around 100 years. The last part of the thesis is devoted to a sensitivity analysis, to evaluate the different effects on activation of the most common and probable impurities, varying their concentration and simulating the effect on the dose.

# Contents

<b>1 Fusion energy: a general introduction.....</b>	
1.1 fusion reactions .....	
1.2 the tokamak layout.....	
1.3 fuel production: TBR concept.....	
1.4 high entropy alloys .....	
1.5.1 A.R.C.: a new tokamak concept.....	
1.5.2 general layout.....	
1.5.3 main focus: the blanket and vacuum vessel .....	
<b>2 Neutronic Simulation and TBR evaluation .....</b>	
2.1 OpenMc software .....	
2.2 geometry definition: D shape single module.....	
2.2 source choice .....	
2.4 structural materials for the vacuum vessel .....	
2.4.1 basic case: Inconel 718 .....	
2.4.2 high entropy alloy .....	
<b>3 Activation analysis .....</b>	
3.1 Fispack -II software.....	
3.2 Activation analysis: Inconel vs high entropy alloys.....	
3.3 Impurity analysis.....	
3.3.1 Activation analysis in presence of impurities.....	
3.3.2 Sensitivity analysis.....	
<b>4 Conclusions.....</b>	

## Bibliography

## List of figures

## List of tables

**Appendix A: OpenMC script example**

**Appendix B: FISPACT-II script example**

**Ringraziamenti**

# Chapter 1

## Fusion energy: a general introduction

The problem of energy supply in our modern, industrial society is becoming harder in the XXI century; science has proven the central role of combustion's emissions in climate change, but the energy consumption increases year by year, while its reduction appears to be not a viable strategy. The development of clean energy options is crucial in this frame, still considering other issues like public acceptability, excessive land usage, waste disposal, technical costs, toxic emissions. Unfortunately, such kinds of problems affect the main two currently available resources, nuclear energy and "renewable sources", i.e., solar, wind or hydroelectric power. These last options suffer different natural limits, which practically prevent their penetration in the energy mix beyond a certain percentage: low energy density, complete reliance on weather conditions (which are not controllable), high cost, large soil consumption or, in the case of hydroelectric, environmental requirements, not available in many countries [1]. For what concern fission energy, it has the capability to produce a huge amount of power with a small land consumption and high capacity factor. Fission reactors regrettably produce radioactive wastes, leading to ad hoc disposal solutions, and suffered some main accidents in the past: the public acceptability of this solution appears to be very low in many European countries. Nuclear fission is also a not-renewable energy; Uranium is well distributed in the earth's crust but some issues on fuel reserves have been raised. Another not negligible problem can be the nuclear proliferation [1]. Fusion energy have the potential for overcoming the limits of fission, still conserving the benefits. Safety issues related to chain reactions will not take place in this frame, as well as greenhouse emissions or, more in general any harmful chemical emission. Not involving Uranium or Plutonium, nuclear proliferation would not be a problem, as well as geological disposal. The storage time for structural materials involved in future tokamak, indeed, is valued in the order of 100 years. Fuel reserve issue can also be neglected for fusion, so that it could be considered as renewable energy. Considering the Deuterium-Deuterium reaction, oceans store enough fuel to power the earth for about 2 billion years at the present rate of energy consumption [1]. Unfortunately, this reaction is the more technically challenging, due to its low cross section. The Deuterium-Tritium reaction is the best candidate to power the first generation of fusion reactors, with the drawback that Tritium must be produced by Lithium breeding.

# 1.1 Fusion reaction

Nuclear fusion reaction is in some sense the opposite of the well-known nuclear fission reaction; while fission involves the splitting of heavy nuclei in lighter fragments with energy release, the fusion regards the merging of light elements in heavier nuclei. In principle many light elements can take part in fusion reactions but fusing smaller nuclei is easier and more convenient from the energetic point of view. For this reason, the fusion of Hydrogen is the main choice. Hydrogen presents 3 main isotopes, Protium, Deuterium and Tritium, with respectively 0, 1 and 2 neutrons; while Deuterium and Protium are naturally present in the natural composition of Hydrogen, Tritium is weakly radioactive with a small half-life, so that it can be found only in small quantities in the high atmosphere [2]. Two nuclei must overcome the coulomb repulsion to merge, being at a very low relative distance ( $10^{-13}$  cm); very strict conditions on temperature, pressure and density are required. Still providing the correct environment, which is technologically challenging, the fusion reaction has a finite, low probability to happen, as presented in the reaction rate graph (figure 1)

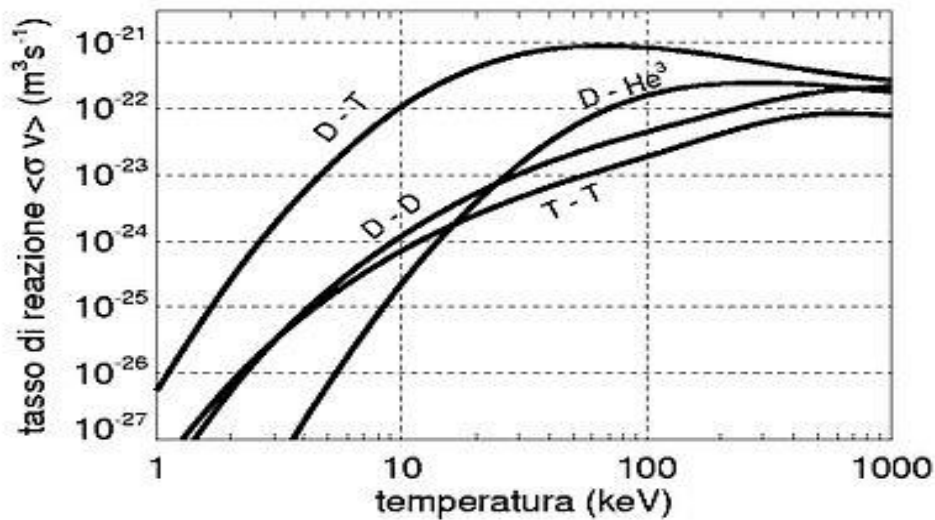
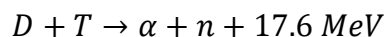
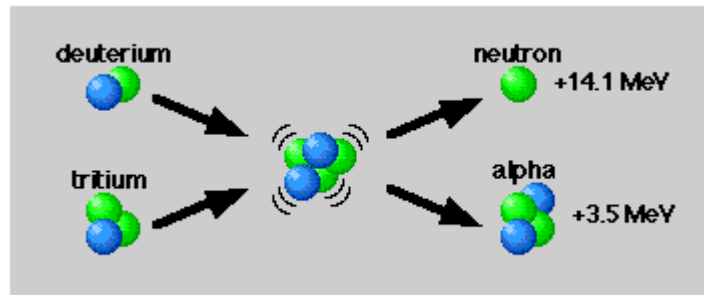


Figure 1 Fusion reaction rate as function of T [3]

Even if the Deuterium-Deuterium reaction is the most interesting from the fuel production point of view (deuterium is minable from the oceans) higher Temperatures are required, adding an unmanageable complexity in the first generation of reactors. For this reason, the more attractive fuel mixture at the present (2022) is a 50-50% Deuterium-Tritium gas, involving the reaction [1]:



The reaction dynamic is schematized in figure 2



*Figure 2 Deuterium-Tritium fusion reaction [4]*

The reaction is exothermic, producing a neutron and a Helium nucleus (alpha particle), releasing 17.6 MeV in the form of kinetic energy. For momentum conservation law the energy is distributed between the particles inversely proportional to the mass; the neutron receives around 4/5 of the energy [1]. As said before, this reaction presents lower restriction on temperature with the drawback of the not negligible issue of tritium production. This aspect will be treated in paragraph 1.3.

## 1.2 Tokamak layout

To obtain fusion reaction Deuterium and Tritium must be kept in a condition of high temperature and pressure for a sufficiently long time, allowing particles collisions. The maintenance of such environment and the issues of avoid unwilled nuclei in the fuel mixture pose the natural problem of fuel confinement, which is clearly not compatible with any kind of physical wall. Due to the high temperature the mix of Deuterium and Tritium for fusion purpose is no longer a gas but a fully ionized plasma; magnetic fields can be used to confine the system, which is basically composed of charged particles. The most studied configuration for a magnetic confining machine is the Tokamak concept, designed in Russia in the '50s of the XX century [1].

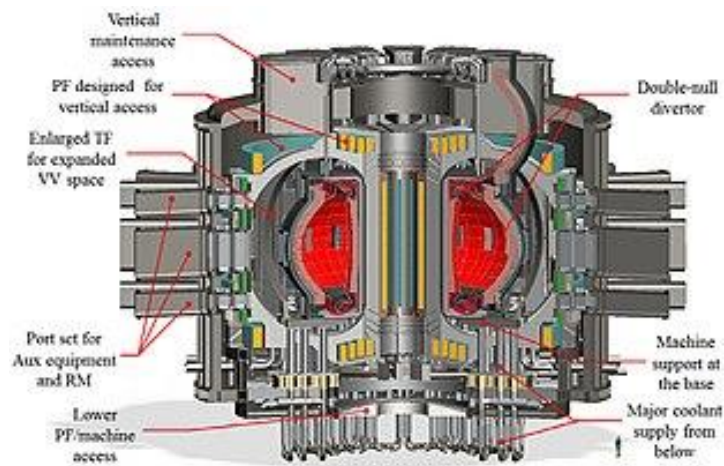


Figure 3 example of a tokamak machine [5]

The main idea is to force the plasma to move in a periodic system, a torus, following magnetic field lines while the desired fusion reactions take place. Neutrons are clearly unconfined by any magnetic field, so they are free to escape from the plasma chamber. Still, they bring the larger part of the energy produced and can be harmful for workers, so a shield around the central torus, the blanket, has the role to stop them, catching their energy for power production; in the blanket neutrons can also play an important role for tritium production, as clarified in chapter 1.3. Alpha particles remains inside the reactor; ideally they could balance the energy losses of the plasma, allowing the so called “ignition condition”, in which external energy is no needed [1]. Unfortunately, a pure toroidal magnetic field is unable to confine a plasma, due to its natural dependence on the major radius. The spatial gradient in a pure toroidal magnetic field leads to drift velocities in particles motion able to destroy the plasma column in few milliseconds. The tokamak configuration needs also a poloidal and a vertical component of the magnetic field to work successfully, as shown in figure 4.

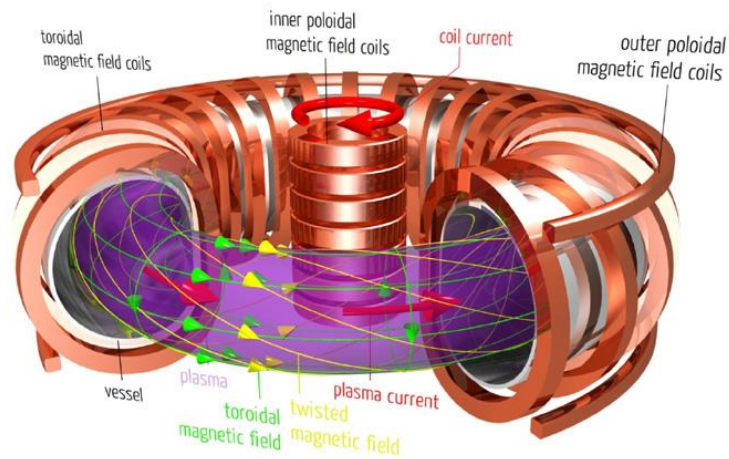


Figure 4 tokamak magnetic fields and coils [5]

The final effect of the superposition of these fields is an helicoidal twist on the toroidal field, able to compensate for drift velocities. The poloidal component of the magnetic field is one of the trickiest aspects of the tokamak layout. While the vertical and the toroidal magnetic field are generated using superconductive coils (toroidally and poloidally), the poloidal component takes advantage of the high electrical conductivity of a fusion plasma. Using the transformer principle, a current is generated in the plasma toroidally, varying the current in the central solenoid. The plasma in the toroidal current, then, is able to self-produce the willed poloidal field, according to the Faraday-Lenz law. The different generation way of each component is sketched in figure 5.

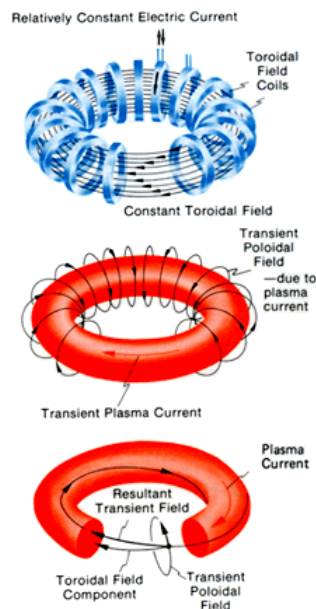


Figure 5 magnetic field components and their generation [5]

The main drawback of the tokamak configuration is linked to the use of the Faraday-Lenz law to produce the poloidal field; transient phenomena are physically required, which are not willable in a system designed to produce energy in a constant manner.

### 1.3 Fuel production: TBR concept

The first generation of fusion reactor will be powered by a 50-50% mixture of Deuterium and Tritium. While deuterium is easily available in nature, the Tritium supply is still an issue. Few quantities of this radioactive nuclide are produced by heavy-water-moderated fission reactors, by deuterium neutronic capture, with an output of around 2 kg/years [7]. Clearly this side production is not enough for power many reactors around the world and the available Tritium inventory, in the worst scenario, could be totally depleted in 2050. The tritium inventory evolution scenarios consider both the usage of the nuclide and the natural depletion due to radioactive decay.

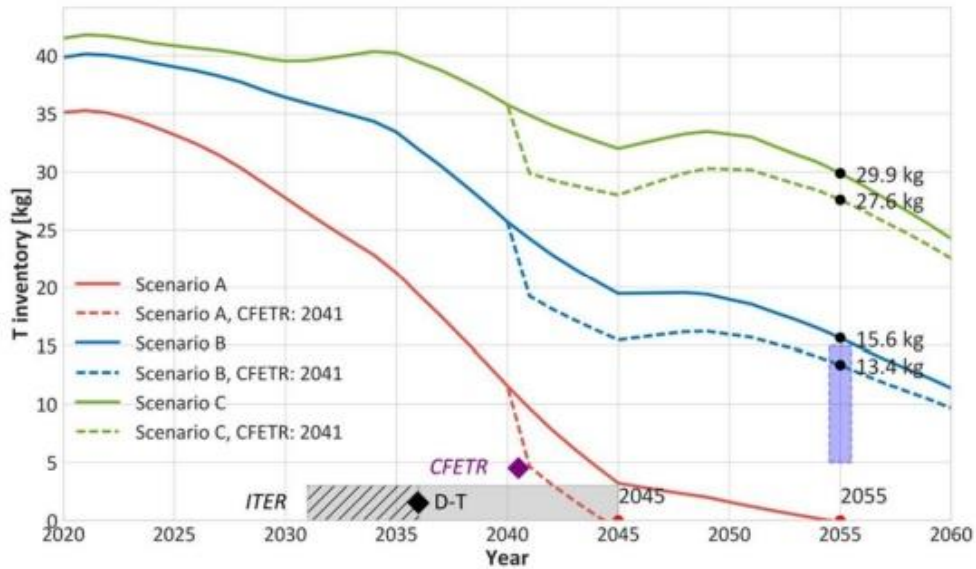
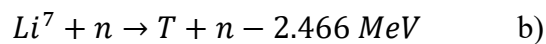
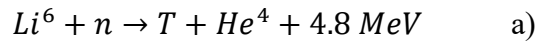


Figure 6 tritium inventory evolution scenarios [6]

To make a general usage of fusion reactors for power production a tritium generation process must be designed. Fortunately, Tritium can be obtained from Lithium, according to the reactions:



Since both the reaction requires the depletion of neutrons, which are generated in the toroidal chamber, the main idea is to exploit the tokamak itself for fuel production, breeding Lithium in a specific component, the “blanket”. To obtain a self-sustained reactor, the blanket should be able to produce a Tritium nucleus for each one burnt in plasma; numerically, this efficiency is expressed by the TBR ratio [7], defined as

$$TBR = \frac{\text{Tritium produced in blanket}}{\text{Tritium burnt in plasma}}$$

Clearly, a TBR strictly equal to 1 would not consider leakages, storage requirements for start-up, etc, so the real constraint is  $TBR > 1$

The natural isotopic abundances for Lithium are  $Li^7 = 92.5\%$ ,  $Li^6 = 7.5\%$  [8]. To reach the required TBR ratio, an enrichment in  $Li^6$  is required, as can be understood considering figure 7

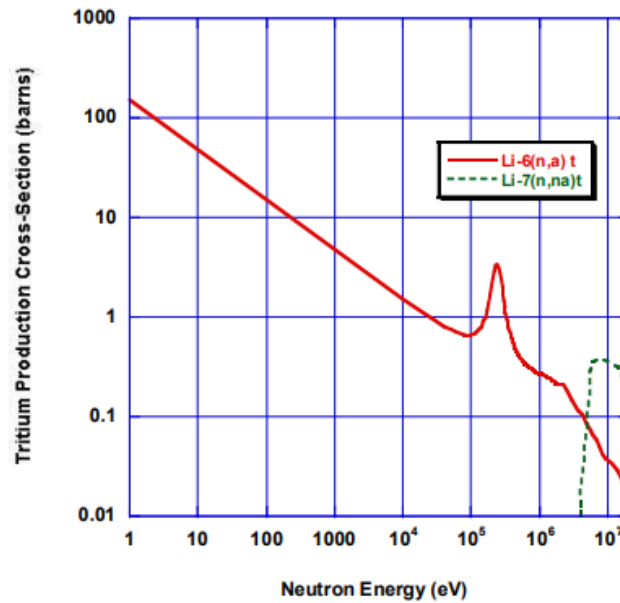
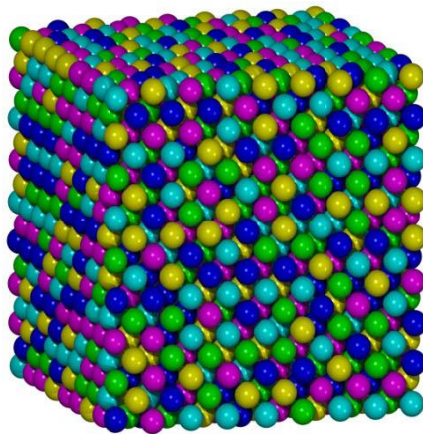


Figure 7  $Li-6(n, \alpha)t$  and  $Li-7(n, n, \alpha)t$  Cross-Section [7]

Reaction b) has the great advantage to produce a new neutron available for another reaction; Still, being endothermic a threshold on neutron energy is present, so that re-emitted particles (as well as slowed down neutrons) could not be able to react. Conversely, the cross section for a) increases at lower energies, giving the chance of exploit a larger part of neutronic spectrum. To fulfil the condition  $TBR > 1$  a neutron multiplier, like the Beryllium, could be necessary inside the blanket. Such materials contain in general traces of Uranium or other heavy nuclides, which can meddle with the requirements on waste disposal and recycling. Due to the great importance of these objectives for public acceptability, large efforts were made to eliminate the multiplier from the reactor. The strategy studied in this thesis is the improvement of the neutronic properties of structural materials, enhancing the TBR consequently. Under this aspect, high entropy alloys are very interesting.

## 1.4 High entropy alloys

Structural materials inside a fusion reactor must satisfy many different constraints, including resistance to very high heat fluxes, resistance to irradiation, low activation, good behaviour with respect of neutron flux for Lithium breeding. The choice is not straightforward and one of the major candidates in fusion field is Inconel-718 [9]. This alloy is well-performing under neutron flux, exhibiting good mechanical and thermal properties and resistance to corrosion; unfortunately, as shown in this thesis a TBR >1.1 cannot be reached in ARC using Inconel-718 without solid neutron multiplier. New materials are required, and the attention of the scientific community is more and more attracted on High entropy alloys and their unusual properties. While common alloys are based on one main element, with traces of others to increase specific properties, high entropy alloys are constituted of five or more basic elements [10]. The concentration of the basic elements should be between 5-35% and trace of others with concentration < 5% can still be added to improve specific aspects. Such materials have a larger mixing entropy than conventional alloys, and the effect of entropy is more pronounced in this case; for these reasons they have been named “high entropy alloys”. When they were proposed, the classical metallurgy knowledge suggested a limited practical value and hard engineering feasibility; they were supposed to develop intermetallic compound and many kinds of phases, ending with brittle microstructures. Conversely, some of them showed high performances for what concern strength/hardness, wear resistance, exceptional high-temperature strength, good structural stability, good corrosion and oxidation resistance, in particular when they are produced in single-phase. As proven in the neutronic simulation in chapter 3.4.2 high entropy alloys can also be designed considering elements able to increase TBR ratio and reach lower levels of activation, avoiding the problem of geological deposition of nuclear waste. The available scientific literature suggests that H.E.A. can also be produced with the current technology. [11]



*Figure 8 structure model of a CoCrFeMnNi alloy [10]*

## **1.5.1 ARC: A NEW TOKAMAK CONCEPT**

The ITER project, with its second step DEMO, represented the main road for fusion power reactors so far; still, the size and the cost of the facilities are high, and the time scale consequently. Starting from this kind of considerations, scientists of MIT and PSFC proposed the A.R.C design, Affordable, Robust and Compact reactor, aiming to reduce complexity and costs for a combined fusion nuclear science facility (like ITER) and to provide a demonstration for fusion pilot power plant. The reactor is a tokamak machine with an innovative design, involving a liquid blanket and newly available REBCO superconductors. All the considerations and the analysis in the present thesis regard a blanket module for ARC.

## 1.5.2 GENERAL LAYOUT

The main purpose for the ARC design is to reduce costs and time in the nuclear fusion research, allowing to reach faster grid-connected reactors. The size of the machine, consequently, had to be minimized, introducing innovative technologies; the REBCO high-temperature superconductors allow to obtain the required magnetic fields with less bulky device, while the usage of a liquid blanket could condense the cooling and the breeding function in a single component [9].

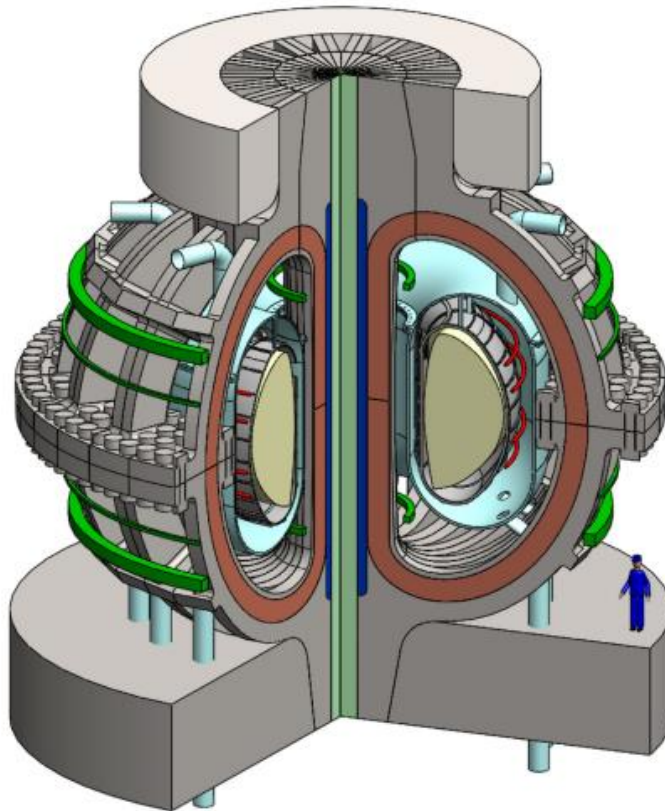


*Figure 9 arc vs man size comparison [9]*

The entire design is characterized by a modular nature; this aspect is fundamental to increase the speed of the project, allowing changes of direction during the experimental campaign without large impact on the device and simplifying maintenance processes. The usage of REBCO superconductive tapes, as well as providing a more intense magnetic field than  $\text{Ni}_3\text{Sn}$ , introduces demountable toroidal coils; they can be split in two parts, for the benefit of modular maintenance. In figures 11-12 main parameters of ARC and ITER are resumed; it appears clear that ARC dimensions are consistently smaller, with a major radius of 3.3 m versus the 6.2 m in the case of ITER; the fusion power is almost comparable, around 500 MW for both the design. This innovative layout of toroidal coils permits to remove the upper part of the machine, to access to the vacuum vessel; it can be considered as a single, replaceable module, externally built and testable. As a first design, Inconel 718 has been chosen for structural material of the vacuum vessel, due to its corrosion resistance, but other materials could be

used in future, as the high entropy alloys presented in this thesis, with higher activation performances [9].

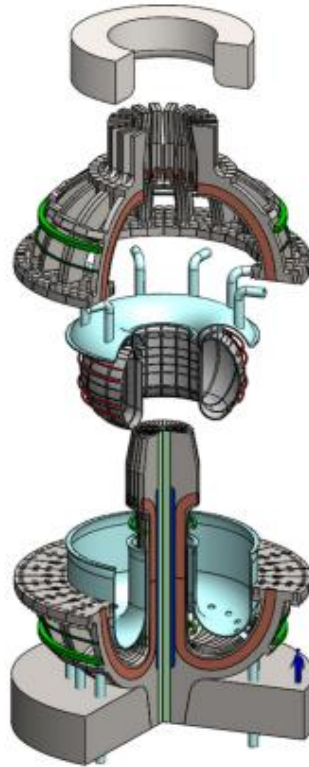


Figure 10a picture of demountable toroidal coils [9]

Design parameter	Symbol	Value
Fusion power	$P_f$	525 MW
Total thermal power	$P_{tot}$	708 MW
Plant thermal efficiency	$\eta_{elec}$	0.40
Total electric power	$P_e$	283 MW
Net electric power	$P_{net}$	190 MW
LHCD coupled power	$P_{LH}$	25 MW
ICRF coupled power	$P_{IC}$	13.6 MW
Power multiplication factor	$Q_e$	3.0
Major radius	$R_0$	3.3 m
Plasma semi-minor radius	$a$	1.13 m
Plasma elongation	$\kappa$	1.84
Plasma volume	$V_p$	141 m <sup>3</sup>
Toroidal magnetic field	$B_0$	9.2 T
Peak on-coil magnetic field	$B_{max}$	23 T
Plasma current	$I_p$	7.8 MA
Bootstrap fraction	$f_{BS}$	0.63
Tritium breeding ratio	TBR	1.1
Avg. temperature	$\langle T \rangle$	14 keV
Avg. density	$\langle n \rangle$	$1.3 \times 10^{20} \text{ m}^{-3}$
On-axis temperature	$T_0$	27 keV
On-axis density	$n_0$	$1.8 \times 10^{20} \text{ m}^{-3}$
Greenwald fraction	$f_{GW}$	0.67
Toroidal beta	$\beta_T$	1.9%
Internal inductance	$l_i$	0.67
Normalized beta	$\beta_N$	2.59
Safety factor at $r/a = 0.95$	$q_{95}$	7.2
Edge safety factor	$q_a$	4.7
Minimum safety factor	$q_{min}$	3.5
Fusion power wall loading	$P_f/S_0$	2.5 MW/m <sup>2</sup>
Energy confinement time	$\tau_E$	0.64 s
H89 confinement factor	$H_{89}$	2.8
H98(y,2) confinement factor	$H_{98,y,2}$	1.8
G89 gain factor	$G_{89}$	0.14

Figure 11 arc main parameters [8]

Parameter	Value
Major radius, $R_0$ (m)	6.2
Minor radius, $a$ (m)	2.0
Toroidal field at $R_0$ , $B_T$ (T)	5.3
Plasma current, $I_p$ (MA)	15
Edge safety factor, $q_{95}$	3.0
Confinement enhancement, $H_{F98}(y,2)$	1.0
Normalised beta, $\beta_N$	1.8
Average electron density, $\langle n_e \rangle$ ( $10^{19} \text{ m}^{-3}$ )	10.1
Fraction of Greenwald limit, $\langle n_e \rangle / n_{GW}$	0.85
Average ion temperature, $\langle T_i \rangle$ (keV)	8.0
Average electron temperature, $\langle T_e \rangle$ (keV)	8.8
Neutral beam power, $P_{NB}$ (MW)	33
RF power, $P_{RF}$ (MW)	7
Fusion power, $P_{fusion}$ (MW)	400
Fusion gain, $Q = P_{fusion} / (P_{NB} + P_{RF})$	10
Non inductive current fraction, $I_{NI} / I_p$ (%)	28
Burn time (s)	400

Figure 12 ITER main parameters [12]

### 1.5.3 MAIN FOCUS: BLANKET AND VACUUM VESSEL

ARC design is characterized by the innovative concept of the liquid blanket, able to condense cooling and breeding function in a single component, thanks to the good properties of FLiBe. This molten salt combines good thermal conductivity and heat capacity, fundamental for cooling functions, neutron multiplication capacity, due to Be presence and tritium breeding, containing Lithium. This configuration implies that the breeding blanket consists basically in a tank filled with FLiBe, surrounding the demountable vacuum vessel and the plasma chamber.

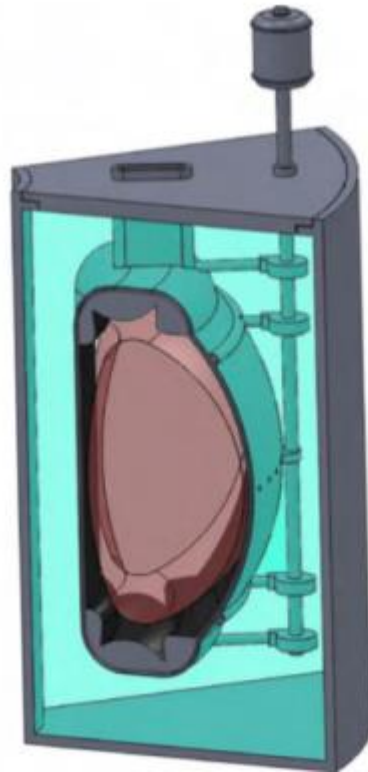


*Figure 13 FLiBe tank surrounding the vacuum vessel [9]*

The pool of FLiBe will provide also a shielding function of fusion neutrons, with its thickness of around 1 meter [9] (transport simulations actually proved that after the first 50 cm larger thicknesses don't provide significant TBR improvements). Since the breeding material is outside the vacuum vessel, its structure is fundamental for tritium production dynamics and the vacuum vessel will face the higher neutron fluxes, with unmoderated particles. It is a double-walled single pieced component, crossed by a FLiBe channel and backed by a Beryllium layer. The presence of Beryllium is in some sense unwilled, because of its price, toxicity, and possible heavy nuclides contamination; still, it is necessary to multiply neutrons before the FLiBe pool. Innovative materials with higher neutronic performances than Inconel can simplify the design guaranteeing the prescribed TBR, as shown in neutronic section of the present work. The plasma-facing layer of the vacuum vessel, the first wall, will be composed of Tungsten; due to the small thickness of this component, the most important consideration for its design is the impact of impurities on the core plasma, while the neutron attenuation aspect is secondary.

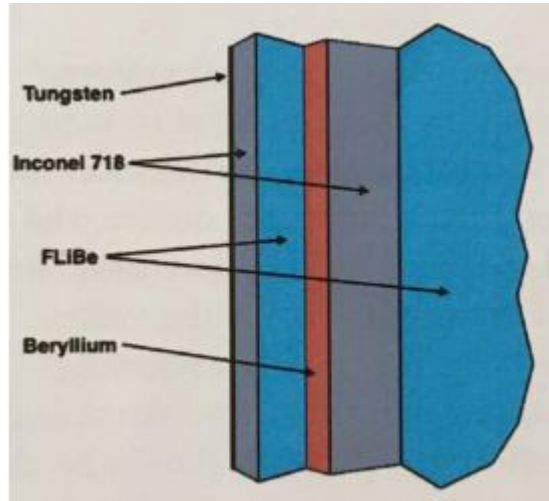


Figure 14 representation of vacuum vessel structure [13]

## **CHAPTER 2**

### **NEUTRONIC SIMULATION AND TBR EVALUATION**

The first part of the thesis consists in transport simulations on the vacuum vessel and FLiBe tank, testing different compositions for the structural layer with a particular focus on Titanium-Tantalum-Vanadium-Chromium-Tungsten high entropy alloys; different papers were published about these alloys, with encouraging results for what concern activation and mechanical properties [14], [15]; a more precise motivation of the choice is provided in chap.2.4. A D-shape model of a single element of the vessel has been generated using the software OpenMC, developed by the MIT; to validate the results, some simulations has been conducted with the original layers of Inconel, obtaining outcomes comparable with the available literature. Eight different high entropy alloys, with different relative composition has been tested, obtaining encouraging results. A TBR larger than 1 has been obtained with all the tested alloys without the Beryllium layer, which can be eliminated from the design; the neutron fluxes obtained from these simulations has been used in chap.3 for activation analysis.

## 2.1 OpenMC SOFTWARE

OpenMC is a neutron and photon Monte Carlo code originally developed by the computational reactor physics group of the MIT; many different universities and labs around the world contribute to it nowadays. It can perform k-eigenvalue, fixed source (function exploited in this work) and subcritical multiplication calculations using models imported by Cad or built by constructive geometry, for both the continuous energy and multigroup transport. From a theoretical point of view OpenMC performs just a regular Monte Carlo transport simulation, describing the behaviour of a particles population using statistics probability. When a particle is emitted (a neutron in this case) the distance of travel before a collision is characterized by a probability distribution; then, when the collision happens, there is an associate probability for each possible nuclear reaction. The streaming of the single particle can be described as a random walk but simulating a large enough number of particles the average behaviour of the population can be obtained. The central limit theorem guarantees that the result can be obtained within an arbitrarily small statistical error. Simulations are performed one particle a time [16]. OpenMC software is based on Python language and a python API is included to enable programmatic pre and post-processing; for installation simplicity a Linux OS has been used to run the simulations (Linux Mint). To perform an OpenMC simulation materials composing the model must be declared; different element and isotopes can be used to compose a single material, specifying their abundances, the density of the whole material and the temperature at which properties must be evaluated. All the defined material must be collected and exported to a XML file, which will be used for the simulation. The model can be declared by constructive geometry; a combination of planes, spheres, cylinders and other forms can be combined to define region of space to allocate different materials, the so-called cells; the union of different cells collected in a root universe builds the model, which must be exported too in a XML file. The geometry can be plotted directly by OpenMC. The next important step is the choice of the source; indeed, simulations for a fusion reactor are of the kind “fixed source”, so that a source must be provided to the model. Many different sources are available, and the user has the possibility to generate a customized source; anyway, in general the main parameters to provide are the energy of the emitted particles, the angular dependence and the spatial distribution. An XML file must be generated also in this case. Then, the general parameter of the simulation has to be set; the user must declare how many particles the software has to run for each batch and how many batches for each simulation. The run mode (i.e. the kind of calculation, like “fixed source” or “k-eigenvalue” etc) must be declared in this section, which again has to be exported in a XML file. In principle at this point the simulation can be ran but the results will be very poor; indeed, the data to be counted have not been declared. The user must set a tally object, declaring which reactions or events have to be counted during the simulation (e.g., absorption, leakages, tritium production and so on). OpenMC scripts support post processing analysis, in which tally results can be mathematically threated or graphics can be generated [16].

## 2.2 GEOMETRY DEFINITION: D-SHAPE SINGLE MODULE

The ARC reactor, as well as other tokamak machines, is expected to be toroidal-angular symmetric, with main differences on neutronic aspects in dependence on the radial and azimuthal angle mainly; consequently, the study can be conducted on a single blanket module, extending the results to the whole system. Preliminary neutronic studies on ARC have been conducted in the past using purely cylindrical models, neglecting the real shape of the plasma chamber [17]; exploiting OpenMC software capabilities in the present work a D-shape model has been constructed, to represent more closely the real geometry of the problem. Considering a single element model, the toroidal curvature is neglected, so that it is linearized with a height of 100 cm, a slice of around 1/8 of the entire component [17]; for what concerns the blanket composition the layout described by Kuang et al. [13] has been followed, substituting in the two structural layers originally composed by Inconel different high entropy alloys. The beryllium layer has been initially considered; then it has been filled with FLiBe, trying to individuate an alloy able to provide a TBR > 1.10 without it, a goal of ARC design. The model obtained is presented in the following figures.

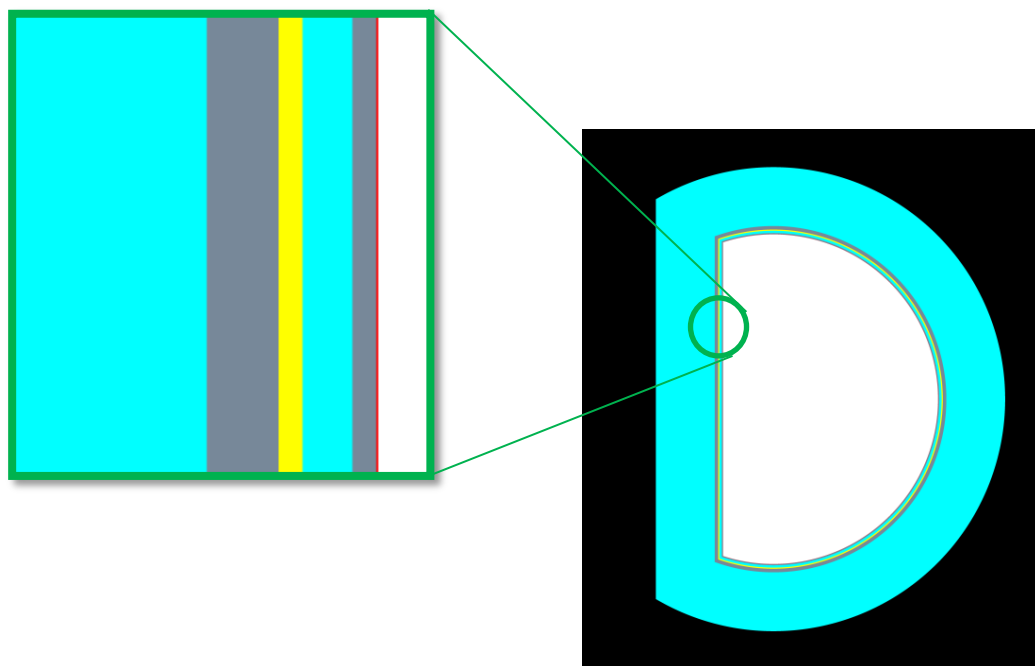


*Figure 15 D model cross section and particular*

A magnification of the model in figure 15 allows to appreciate each layer; the tungsten first wall is represented in red, the two structural layers in grey, the beryllium neutron multiplier in yellow and in light blue the FLiBe. Notice that the external FLiBe pool thickness has been reduced to 50 cm, as suggested in [17]. The thicknesses of each layer are resumed in table 1; it is important to notice that the model is obtained combining planes and cylinders, with a basic internal cylinder of radius 1399 mm.

*table 1 thicknesses of each layer*

<b>Layer</b>	Tungsten	Structural layer 1	FLiBe channel	Beryllium	Structural layer 2	FLiBe pool
<b>Thickness [mm]</b>	1	10	20	10	30	500

## 2.3 SOURCE CHOICE

Many different sources are available in OpenMC to simulate the presence of plasma in the chamber; in general neutron emission can be considered isotropic and consequently point like sources or isotropic box sources located on the axis have been used in past [17]. Anyway, recently OpenMC released a new package with different customized fusion sources [18], in which physical parameters can be set to reproduce closely the plasma conditions in a specific reactor. In the present work this source model has been used; the physical parameters chosen, mainly obtained by the work of Sorbon et al. [9] are presented in table 2

*table 2 source set parameters [9]*

<b>SOURCE CHARACTERIZATION</b>	<b>VALUE</b>
Elongation	1,84
Ion density centre	1,80E+20
Ion density peaking factor	1
Ion density pedestal	1,05E+20
Ion density separatrix	1,00E+20
Ion temperature centre	27
Ion temperature peaking	8,06
Ion temperature pedestal	2,5
Ion temperature separatrix	0,5
Major radius [cm]	330
Minor radius [cm]	60
Pedestal radius	0,8*20
Mode	H
Shafranov factor	0,44789
Triangularity	0,27
Ion temperature beta	6

The tokamak source used constitutes in a toroidal plasma column, with a curvature radius despite the D module is straight; the geometry anyway is set such that the source is contained without touching any wall, and the plasma column is automatically cut at the sagittal boundary of the model; here a reflective boundary condition has been stated, simulating the continuity of the torus. A sketch of the source is presented in figure 16; in figure 17 the source is inserted inside the geometry of the problem.

Neutron source density 3D

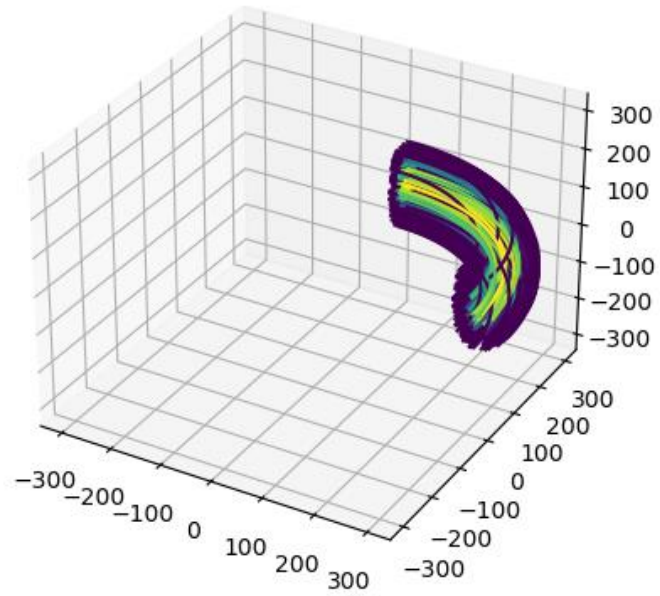


Figure 16 tokamak source neutron density

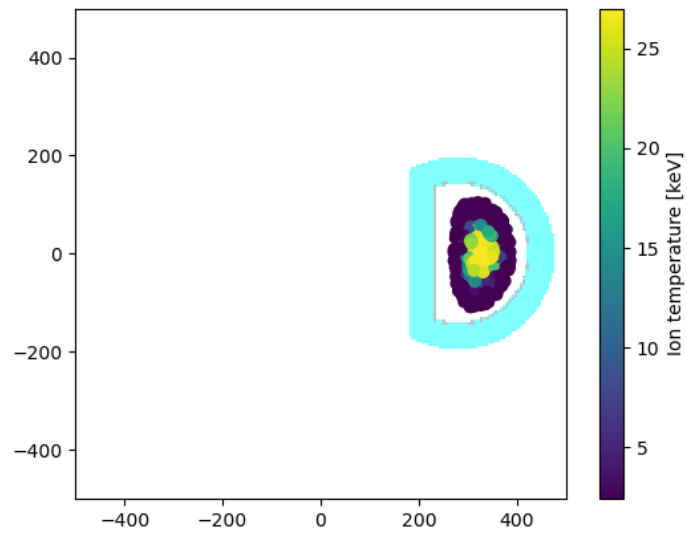


Figure 17 cross section of the source located inside the D model: ion temperature representation

The physical parameters of the plasma column can be plotted directly by the package; the profile of the neutron source density is represented in figure 18, while the ion temperature profile is presented in figure 19. It is important to notice that at the present level of design the plasma parameters for arc are just supposed.

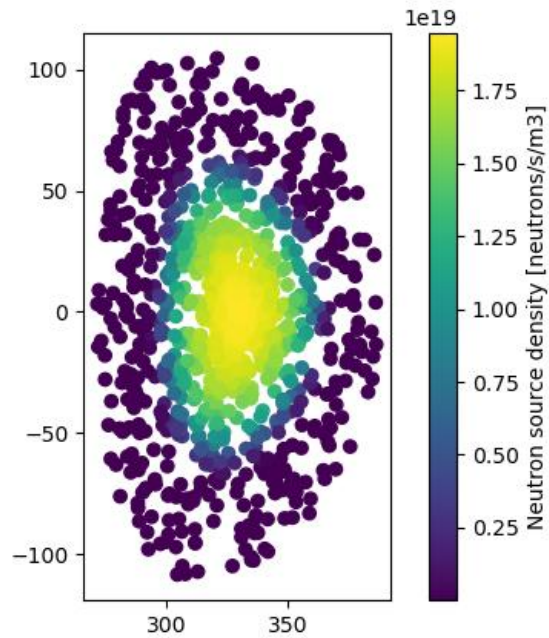


Figure 18 tokamak source neutron density profile

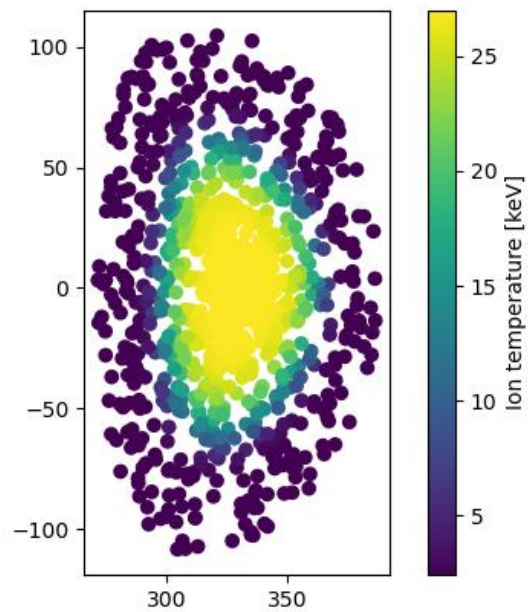


Figure 19 tokamak source ion temperature profile

## 2.4 STRUCTURAL MATERIALS FOR THE VACUUM VESSEL

Inconel 718 has been presented as baseline structural material for the vacuum vessel, due to its resistance to corrosion and strength in high temperature environments [9]; these properties rely mainly on the Nickel content, with the drawback of nuclear activation. Precise composition of Inconel 718 is listed in tab 3. Anyway, further iterations on the vacuum vessel materials are expected [9] thanks to the modular nature of the design and V-Cr-Ti alloys have been considered [17], proving their superiority for what concern nuclear activation. On the other hand, W is considered as a reference material for plasma-facing components, despite some limitations due for example to radiation induced embrittlement; still, W properties are of an extraordinary interest in fusion applications and intense research has been conducted to improve its characteristic combining many elements in new alloys. The combination of W in high entropy alloys provided the most interesting results, including enhanced mechanical strength even at high temperatures, oxidation resistance, fatigue and high-temperature fracture resistance, good thermal stability and toughness [14]. Trying to produce material for fusion application, neutron activation resistance is one of the most important properties: Cr, V, Ti, Ta were selected from the most commonly used refractory metals for this reason. In particular, Ti increases the sintered density through interdiffusion, V improves strength and hardness of the alloy, Cr was chosen to exploit its capability of induce passivation [14]. Starting from this result and considering the great performances of high entropy alloys, in this work a V-Cr-Ti-Ta-W alloy will be tested, starting with an equimolar composition, the basic formulation for this kind of materials. The presence of V-Cr-Ti and the elimination of Ni should guarantees better performances on Inconel for the activation aspect, which will be treated in cap.4. The presence of beryllium as a neutron multiplier still is an issue, due to its cost, toxicity, contamination and for the waste production; high entropy alloys could allow its elimination, so different compositions will be tested, trying to optimize TBR without a multiplying layer. Eight compositions, listed in table 4, have been proposed and simulated. The density of each composition was calculated as the average of the elementary components density, weighted on the mass fraction.

*table 3 Inconel 718 composition, % in mass [19]*

Element composition	Ni	Cr	Fe	Nb	Co	Mn	Cu	Al	Ti	Si	C	S	P	B
Inconel 718	50	17	18.5	4.75	1	0.35	0.2	0.65	0.3	0.35	0.08	0.015	0.015	0.006

*table 4 High Entropy Alloys compositions*

<b>COMPOSITION</b> <b>%</b>	<b>BASE</b>	<b>A</b>	<b>B</b>	<b>C</b>	<b>D</b>	<b>E</b>	<b>F</b>	<b>G</b>
V	20	30	40	60	20	30	30	20
Cr	20	10	5	5	5	10	5	2,5
W	20	40	40	20	60	30	30	70
Ta	20	10	10	10	10	20	30	5
Ti	20	10	5	5	5	10	5	2,5
density [kg/m3]	10.7314	12.36	12.39	9.76	15.02	12.1	13.19	15.82

## 2.4.1 BASIC CASE: INCONEL 718

To validate the model comparing results with the available literature and to have an element of comparison for the high entropy alloys, preliminary simulations have been conducted considering Inconel 718 as structural material, with and without the Beryllium layer. In both the cases the simulation involved 30 batches plus 10 inactive, running 10 000 particles for each batch; the temperature of the model has been set at 900 K as reference temperature.

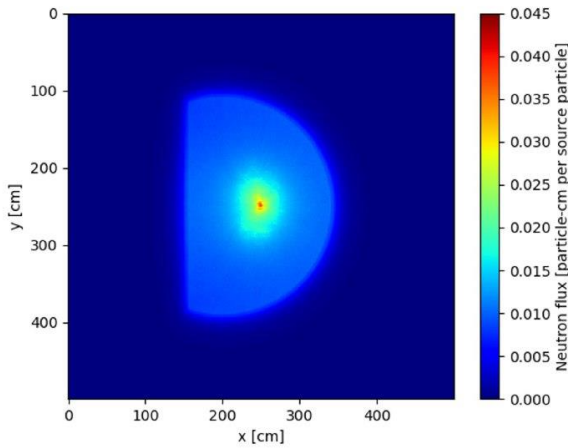


Figure 21 Flux distribution, Be layer, Inconel 718

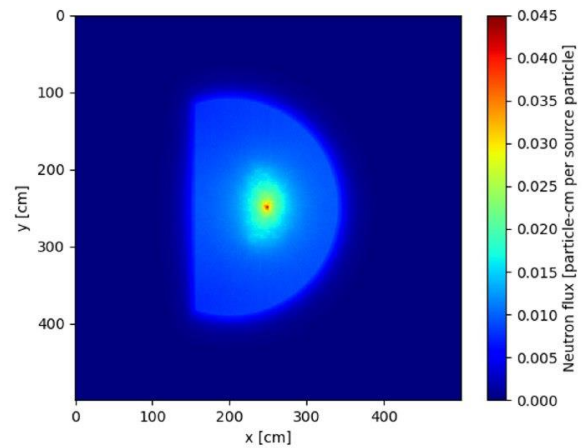


Figure 20 Flux distribution, no Be layer, Inconel 718

The flux distribution in the system with and without the beryllium layer is presented in figures 20 and 21; the differences are not easy to appreciate but relevant effects are present in total TBR production. In figure 22 and 23 the tritium production spatial distribution is presented; in figure 23 the Be layer has been filled with FLiBe, practically increasing the size of the breeding-cooling channel.

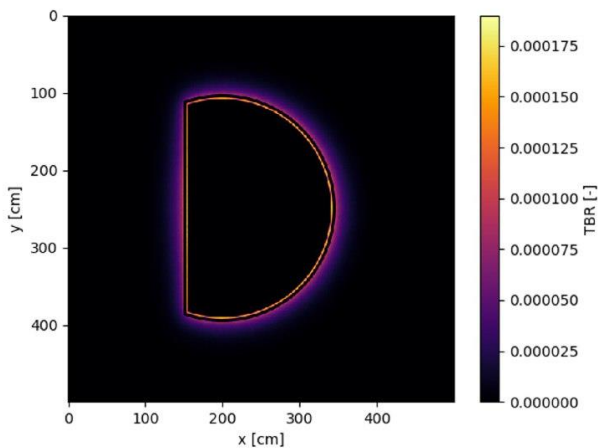


Figure 23 TBR mean value, Be layer, Inconel 718

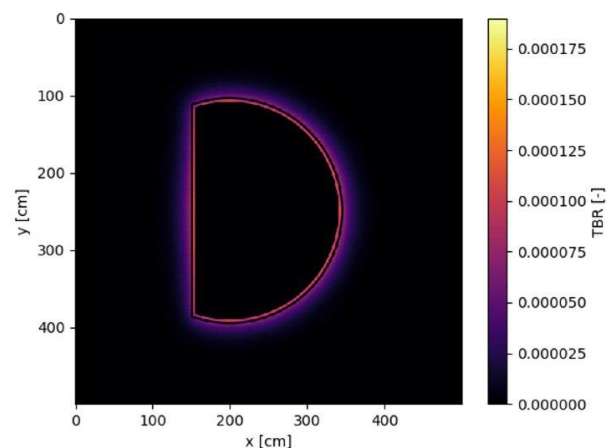


Figure 22 TBR mean value, no Be layer, Inconel 718

Looking at the images it appears clear that increase the size of the FLiBe channel is not enough to compensate the remotion of the neutron multiplier and the final result is a general decrease of tritium production. The choice of limiting the thickness of the external FLiBe pool at just 50 cm is also justified, since the H production decreases quite faster after the first 20 or 30 cm. In figure 24 and 25 the standard deviations associated to the mean TBR are also presented.

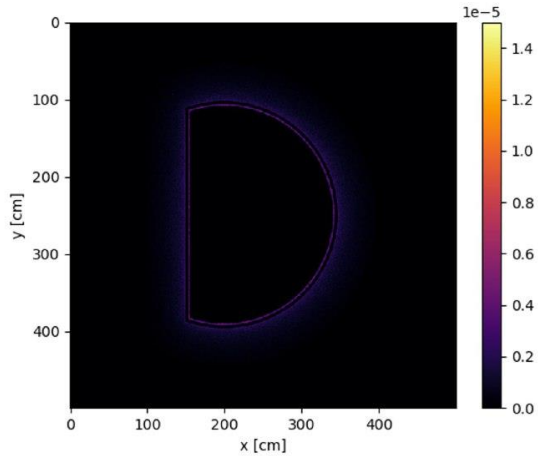


Figure 25 standard deviation, Be layer, Inconel 718

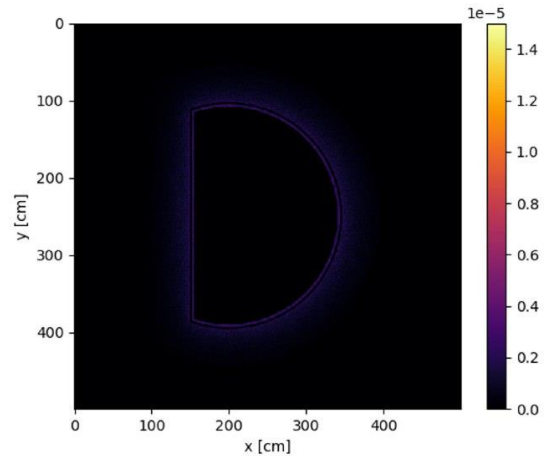


Figure 24 standard deviation, no Be, Inconel 718

The usage of Inconel as structural material allows the system to reach a TBR larger than 1 in both the configuration, as shown in figure 26; here the total TBR is shown as obtained by cell tally on FLiBe filled regions. Anyway, leakages and dispersion must be considered, so that a more conservative limit is to require a TBR > 1.1 (this threshold is underlined by the red line), not feasible also using a neutron multiplier.

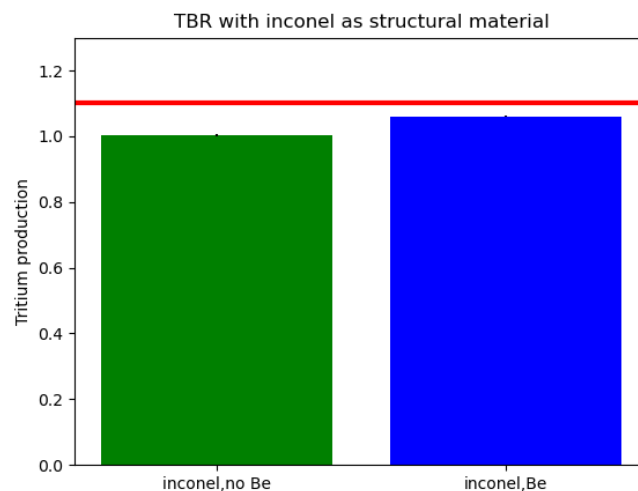


Figure 26 total TBR with and without beryllium layer

In table 5 the total TBR and the relative standard deviations are resumed.

table 5 TBR and standard deviations; Inconel 718 as structural material

layout	TBR	Standard deviation
Inconel, Beryllium layer	1.062	0.0028
Inconel, no Beryllium layer	1.002	0.0033

The increasement of the size of the first channel of FLiBe is not able to increase the tritium production in this layer, while it causes a strong drop in the TBR fraction obtained in the pool region, as it is shown in figure 27; the amount of tritium produced here, furthermore, is dominant on the total.

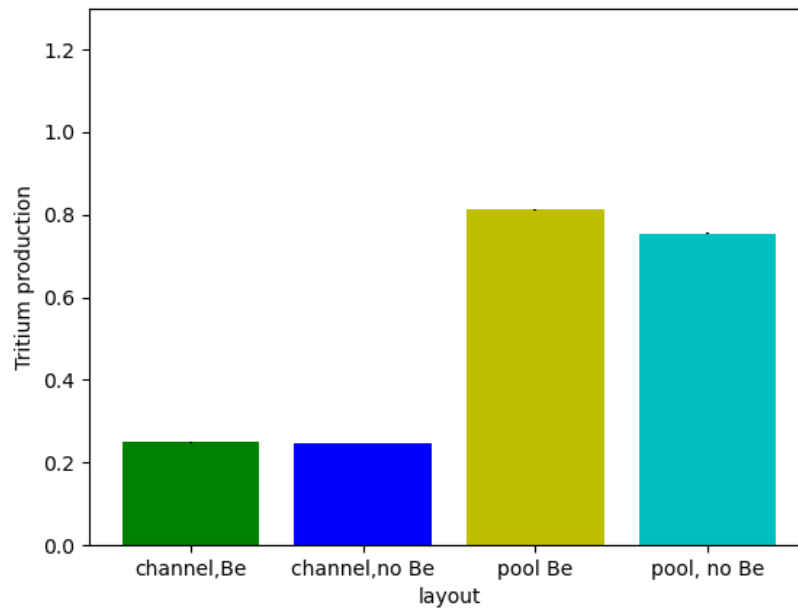


Figure 27 fraction of Tritium production in the channel and in the tank

The precise fraction of each layer in both the configuration is listed in table 6.

table 6 precise T production fraction in each layer

Layer and configuration	T production fraction	Standard deviation
Channel with Be layer	0.2490	9E-4
Channel, no Be layer	0.2463	1.2E-3
Bulk with Be layer	0.8126	1.67E-4
Bulk, no Be layer	0.7540	1.66E-3

## 2.4.2 HIGH ENTROPY ALLOYS

As presented in table 4, 8 different compositions for the V-Cr-Ti-Ta-W alloy have been considered and tested; seen the encouraging results with other V-Cr-Ti alloys in terms of TBR [19] the simulations were conducted directly without the Beryllium layer, filling its space with FLiBe; the reduction of Be inventory indeed is an important goal for activation and safety issues. The source adopted was the tokamak source presented in cp. 3.3 and 50 000 particles have been simulated for each batch, running 30 batches (and 10 inactive batches), reaching a standard deviation of the order of  $10E-3$  on total TBR measured with cell tally. The reference temperature of the model was again 900 k. To provide an upper limit on the breeding capability of high entropy alloys, W was considered as fully enriched in W-184, which is associated to higher neutron multiplying cross section. To compare the performances of different compositions a loop routine has been set in OpenMC, collecting the results in vectors, and saving the neutron fluxes for activation analysis. As shown qualitatively in figure 28 and resumed in table 7, all the proposed alloys satisfy the requirement of  $TBR > 1.1$  without solid neutron multiplier, with higher result for alloy G, able to overcome 1.2 and alloys D, reaching 1.19.

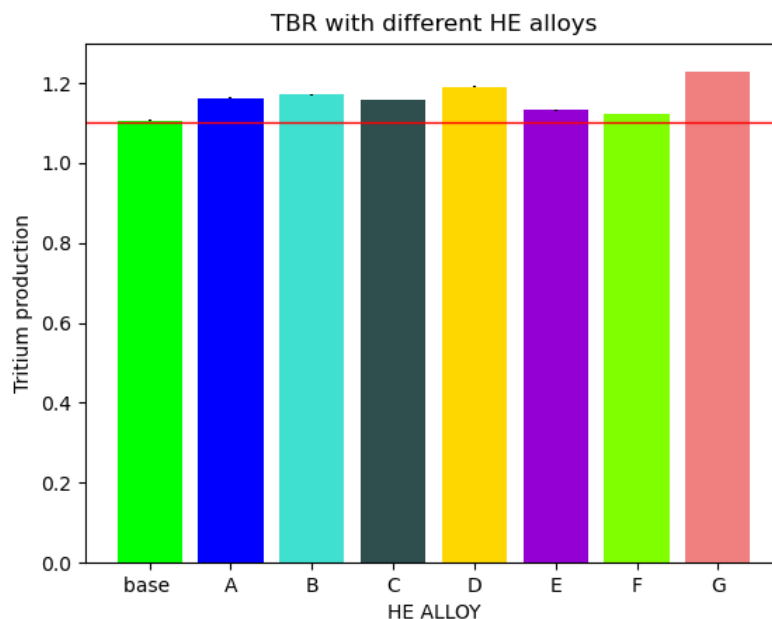


Figure 28 TBR obtained with 8 different high entropy alloys

To identify the most important parameters responsible for higher TBR different aspects have been considered; the density could be an important player, so its role has been investigated. In figure 29 the TBR of each of the 8 alloys have been plotted in function of the relative density. The higher TBR corresponds to the higher density, and in general the TBR seems to increase with density. Anyway, a clear dependence is not identifiable; the lightest alloy present higher performances than E, F and base alloy, which are heavier, and the alloy F, the third heavier in absolute is related to one of the worst

breeding results. The  $R^2$  parameter associated with the least-squares fit model, equal to 0.294, confirms the weakness of the dependence.

table 7 High Entropy Alloys with relative TBR and standard deviation

Alloy	TBR	Standard deviation
Base	1.106	0.0012
A	1.162	0.0012
B	1.171	0.0014
C	1.158	0.0014
D	1.191	0.0014
E	1.132	0.0014
F	1.123	0.0014
G	1.228	0.0014

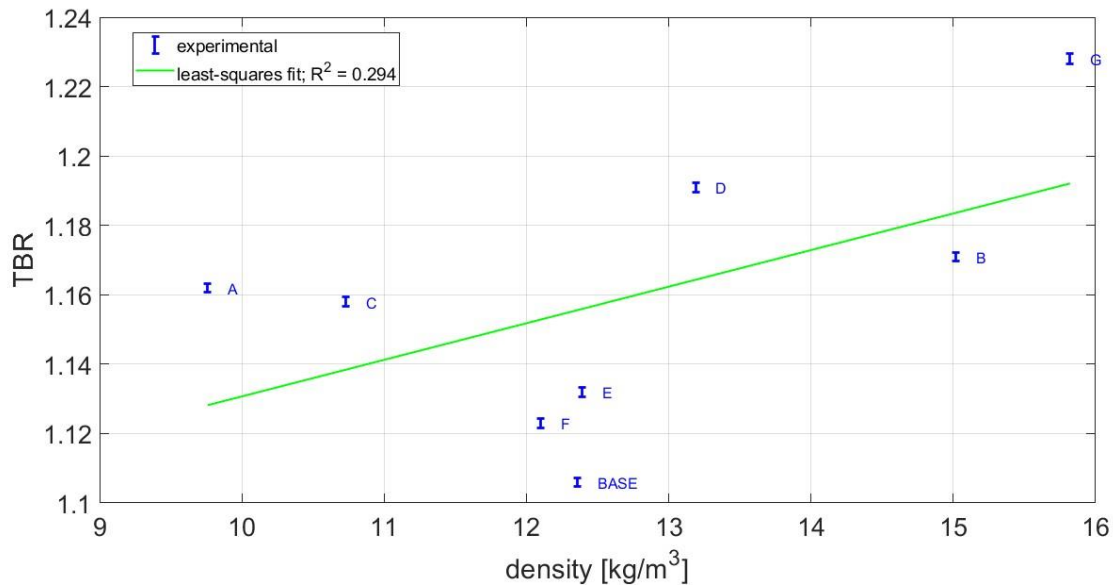


Figure 29 TBR as function of alloy density

Clearly, the density of an alloy is related to its composition and the relative abundances of the five components in the eight tested materials were quite various. The mass fraction of each metal should have a strong effect on nuclear results and on neutron attenuation or multiplication, so a sort of sensitivity on this aspect has been tried. The sensitivity in this case is not rigorously correct, since the

% fraction of each element does not vary while the other are fix; it is more a qualitative test on the impact of the abundance of a certain nuclide on each alloy. The TBR in function of the fraction of V content is shown in figure 30; for the same fraction of V

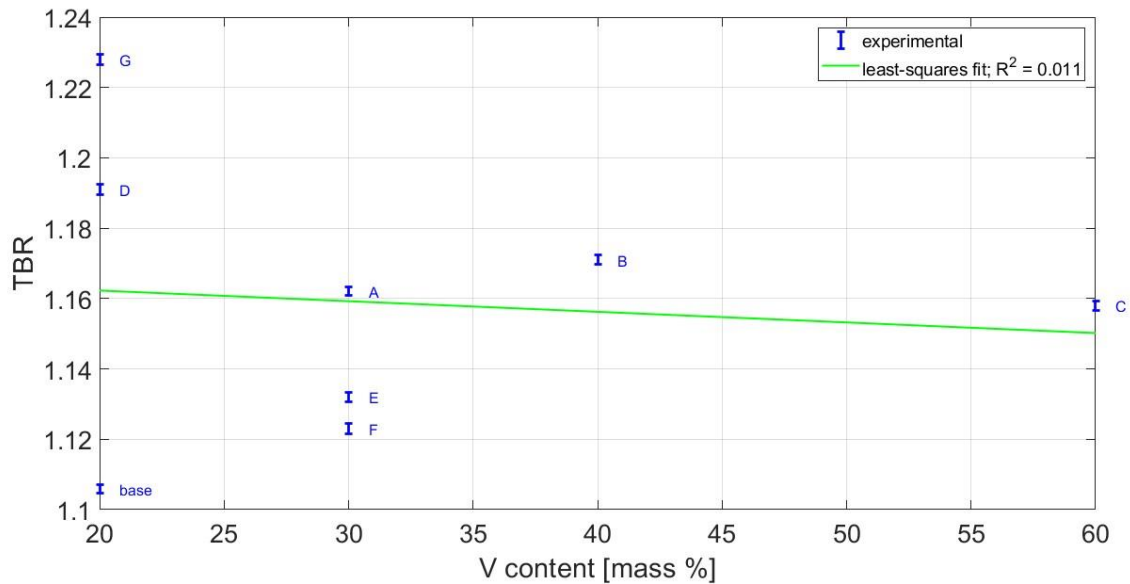


Figure 30 TBR as function of V fraction

the relative TBR are quite various but in general the effect seems to be negative; for this case, anyway, data are very dispersed, so that if a correlation exists it must be totally secondary respect to other dependencies, as proved by an  $R^2$  parameter equal to 0.01, the lowest obtained and very low in general. The Cr fraction, in fig 31, presents negative correlation: the highest presence of Cr in the base alloy, 20% in mass, is related to the poorest performances in terms of breeding, while the most interesting alloy, the G, is again associated to the lowest Cr fraction and the highest W fraction, as can be noticed in figure 32; the  $R^2$  associated with the regression curve is equal to 0.501. The correlation between W fraction and TBR is the most pronounced in absolute, with a clearly increasing trend; this behaviour can depend on the capability of W of multiply neutrons, reducing the neutron flux attenuation in the structural layers; the  $R^2= 0.792$  is the highest value obtained, confirming the important impact of W fraction. The correlation with the Ta fraction (figure 33) appears to be negative, with the highest performances of alloy G associated to the lowest Ta concentration (2.5%); the model in this case presents an  $R^2 = 0.681$ . A similar but less pronounced negative correlation is associated to the Ti fraction; the base alloy, with the highest Ti content produces the worst TBR while the best performance is related to the lowest Ti fraction in G. For the same content of Ti, as in alloys D,B,C and F the most relevant parameter is again the abundance of W; indeed the allow D, the second for W content, is associated with the second higher TBR. The least-squares model in this case is associated to an  $R^2=0.501$ .

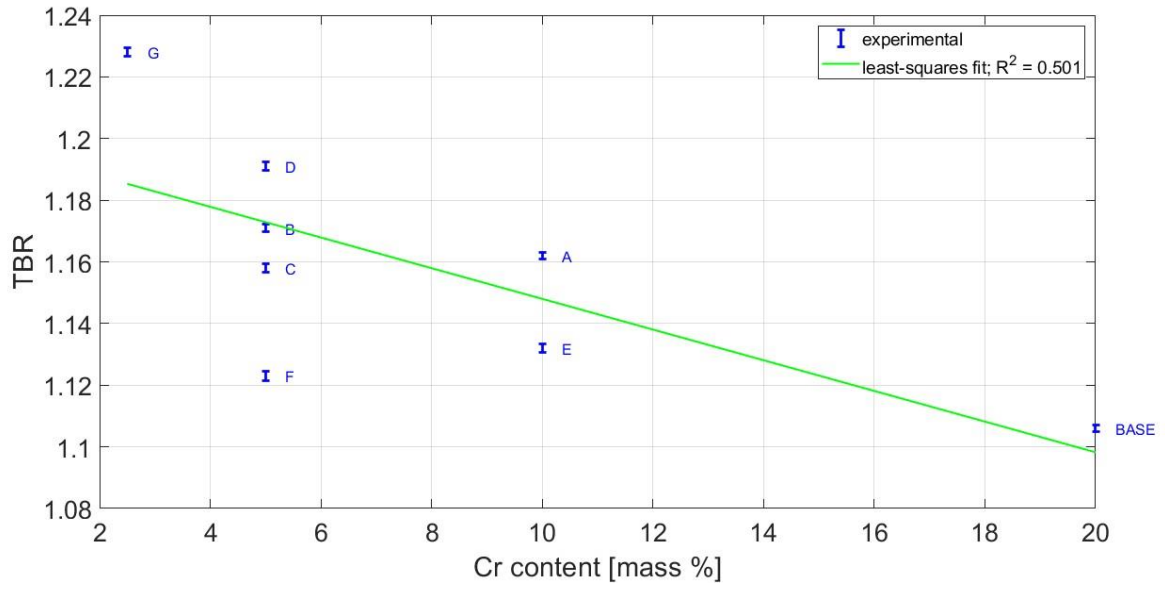


Figure 31 TBR as function of Cr fraction

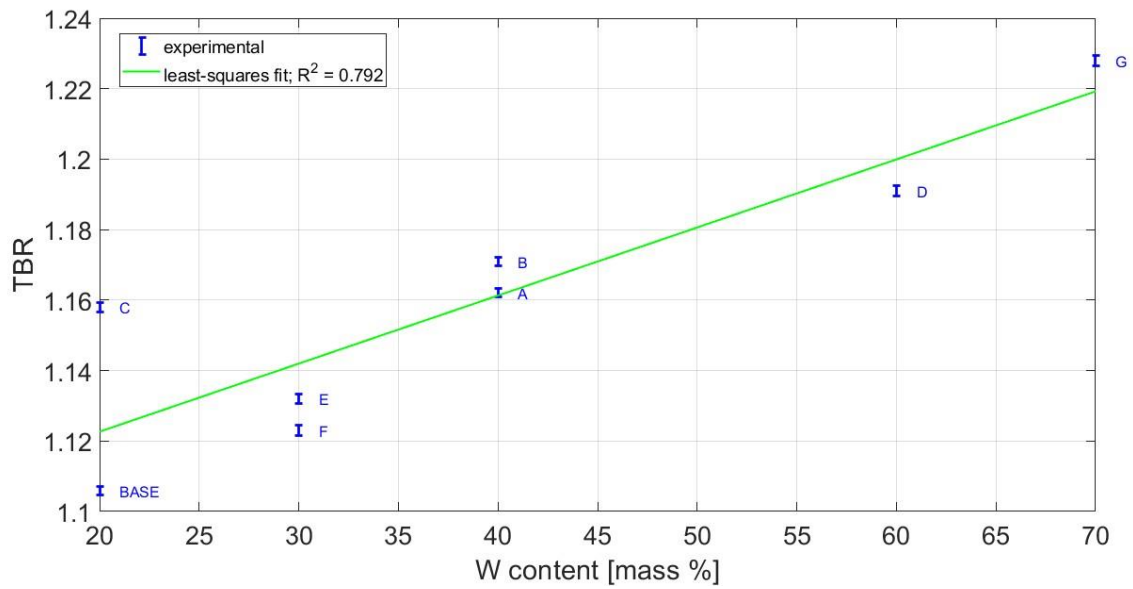


Figure 32 TBR as function of W fraction

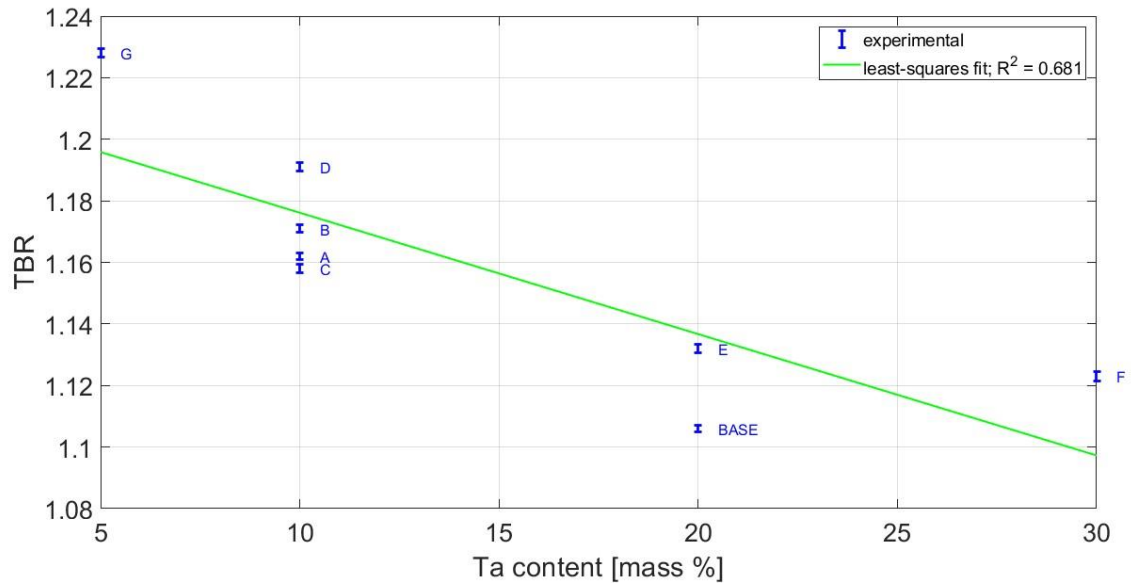


Figure 33 TBR as function of Ta fraction

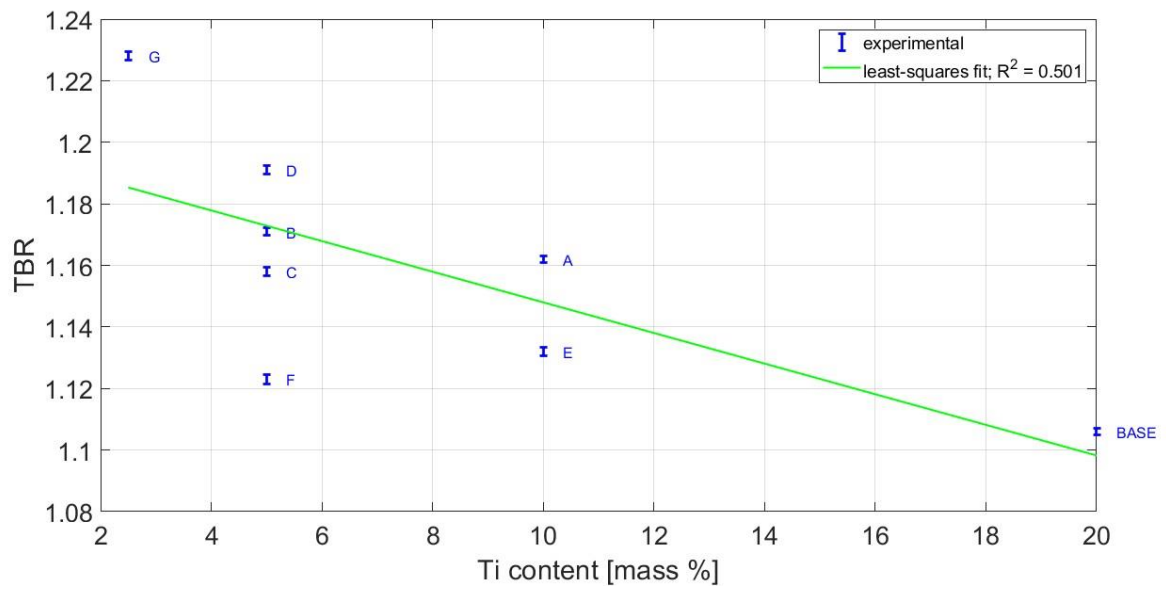


Figure 34 TBR as function of Ti fraction

The most interesting high entropy alloy is the G, so the main results of that simulation are presented below; in figure 35 the neutron flux is plotted in a cross section of the model; figure 37 and 36 show the TBR spatial distribution and the relative standard deviation.

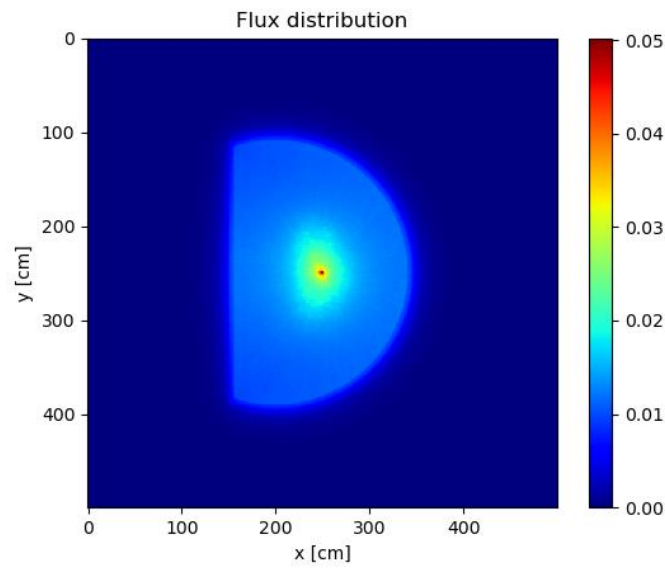


Figure 35 flux distribution , High Entropy Alloy G

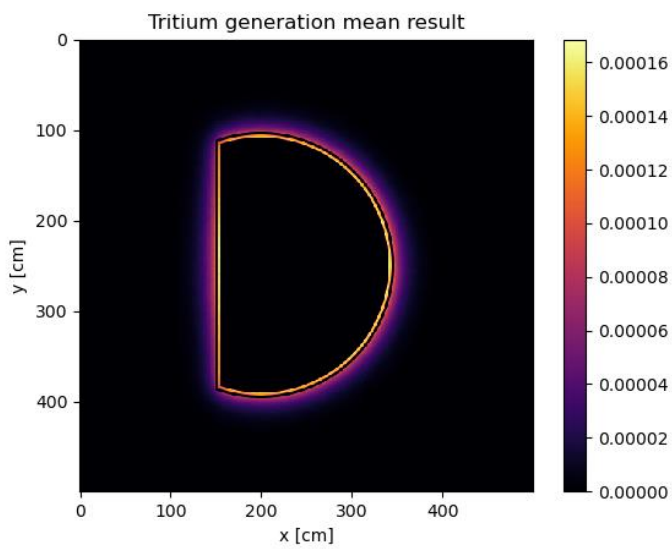


Figure 37 TBR distribution, High Entropy Alloy G

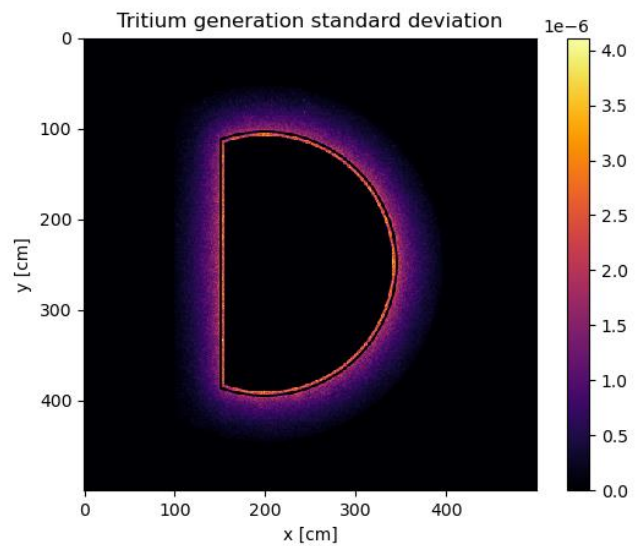


Figure 36 TBR standard deviation, High Entropy Alloy G

## CHAPTER 3

### ACTIVATION ANALYSIS

One of the main reasons for the concern about nuclear energy in the population is the activation of materials and the need for long-time waste deposition; consequently, one of the main goals for ARC design is to lower as much as possible the activity of materials and to avoid in general high level nuclear waste. The reduction of nuclides like Ni in the structural materials, prone to neutron activation and abundant in Inconel 718, is necessary in this frame and high entropy alloys can give an important contribution.

To steer the research correctly the first important step is to define a clear classification for ‘low activation materials’ and limits on dose and decay time must be set. In the present work the limits indicated in [20] will be adopted, considering that these thresholds should be reached in at most 100 years. The focus is on the possibility of recycling the materials after the prescribed 100 years “inside the plant” (which means according to the nuclear field limits) or “outside the plant” (following the limits of general industry); the proposed references are

- Dose rate of  $1e-5$  Sv/h as limit for recycling “inside the plant”; it is deduced from the US annual dose limit for nuclear workers, 20 mSv/y, which equals to  $1e-5$  Sv/h, assuming 8 working hours per day and 5 days per week

- Dose rate of  $1e-6$  Sv/h as limit for recycling “outside the plant”; it is deduced with the same procedure as before, considering the 1 mSv/y regulatory limit for non-nuclear workers, assuming contact time limited to normal working hours

*table 8 Recycling limits*

CONDITION	“In plant recycle”	“Outside recycle”
LIMIT	1E-5 Sv/h	1E-6 Sv/h

## 3.1 FISPACT-II SOFTWARE

To simulate the behaviour of structural materials after the irradiation the validated FISPACT-II software, developed by UKAEA has been used, taking the fluxes provided by OpenMC as input data. FISPACT-II is an object oriented, Fortran based code, able to perform simulations for both charged and neutral particles; in particular, it is a powerful practical activation-transmutation engineering prediction tool. It can extract, reduce and store nuclear and radiological data from the ENDF library files, construct and solve rate equations to determine the time evolution of the inventory in response to different irradiation scenarios (e.g., cooling only simulations, multi-projectile simulations...), compute and output derived radiological quantities and perform auxiliary calculations to identify the key reactions and decays [ 21]. To perform a FISPACT-II simulation 7 files are required as input, collected in the same directory:

- **fluxes**: a file containing the energy spectrum of neutron flux, computed using 709 energy groups, from 1.0471E-5 eV to 1.0000E+9 eV.
- **files.i** : it contains a mapping of physical directories and files to the input and channels for all inputs that FISPACT-II will require for the simulation
- **collapse.i** : a file containing information to reduce each cross-section to a single value by taking the energy-dependent integral with the provided spectrum of the incoming projectile flux
- **condense.i** : a file containing information to condense decay and fission data
- **Print\_lib.i** : a file which uses the binary files containing cross section and decay data generated by the collapse and condense runs to generate a library summary print
- **Inventory.i**: a file containing information on the initial condition of the system, on its composition and on the irradiation and cooling phase to be simulated.

From the user point of view the **inventory.i** file is the most important. Here, the mass amount of the material to be analysed has to be declared, as well as the mass fraction of each constituent nuclide, the material density, the threshold indicating the minimal concentration that a certain nuclear species has to have to be considered in the output and tolerance limits. In this file the graphs to be generated are also declared, indicating which quantities should be computed (e.g., dose, activity, heat output...). The last part of the file is devoted to the declaration of the irradiation phase and of its duration, with the definition of the total flux and of the cooling phase, in which the inventory decays. Time steps at which output the inventory cooling status must be provided, in seconds, minutes, week, months or years.[21]

## 3.2 ACTIVATION ANALYSIS: INCONEL 718 VS HEA

To run the activation simulation using FISPACT-II the neutron fluxes obtained in the neutronic part must be used as input; the neutron flux has been computed with 709 energy groups, as requested by FISPACT-II. An important caveat providing these files from OpenMC regards orientation of the vector; FISPACT-II starts from the most energetic group to the least, while OpenMC saves the data backwards. The flux file must be flipped and a “1.0” must be inserted in the last position, to end the reading procedure of FISPACT-II. The activation analysis was performed for the Inconel 718, as reference case, and for 4 different high entropy alloys: the equimolar Base alloy, A, C, G. The alloy G was chosen for its high performances, A for its composition similar to the base alloy and C for its high fraction of vanadium. To obtain results as precise as possible for each alloy the corresponding neutron flux was used, as reported in figure 38

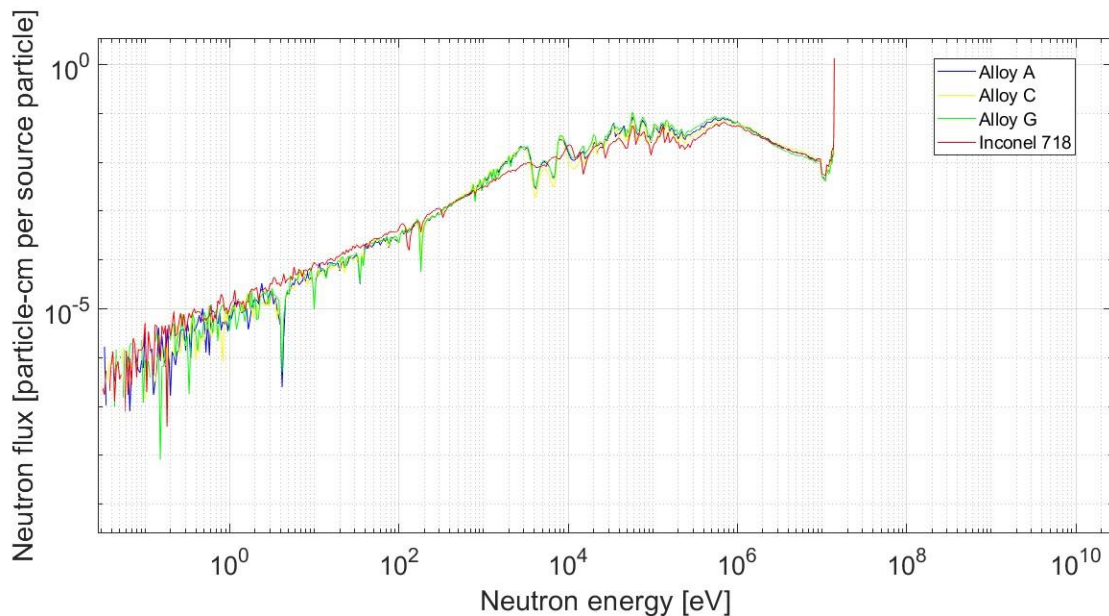


Figure 38 neutron flux normalized on the source

Since neutrons are emitted at 14 MeV and they cannot be slowed down too consistently, a double logarithmic scale has been used to better visualize the trend. The neutron flux is quite similar in all the 4 cases at least qualitatively. As a first approximation a single flux could be used to test different structural materials; anyway, the precise flux has been used for each simulation. For the irradiation phase the approach of [20] was followed, simulating 1 year of continuous irradiation with a total neutron flux of about  $7\text{-}8 \text{ E}14 \text{ neutrons/cm}^2/\text{s}$ . In the first analysis the alloys have been considered pure, with the composition listed in table 4. The results of the simulation are presented in terms of activity, heat output and dose rate, in figures 39,40,41,42. The limits listed in table 8 are indicated by lines on each graph. The high entropy alloys clearly demonstrate their superiority in terms of activation response on the Inconel, already in the short term; after around one year of decay, the HEA and the Inconel curves starts to diverge considerably. As can be seen in figure 39, any of the different HEA tested can be considered as “low activation materials” in general, with an average reduction of the dose on the Inconel of around 5 orders of magnitude after a century. A focus on the dose is

presented in figure 40; all the proposed composition allows an “in plant recycling” after 100-200 years, with best performance obtained by alloy G, which is also associated with the highest TBR ( 123 years for alloy G, 180 years for the base alloy); The “outplant recycling” goal, furthermore, is achieved by all the alloys in 300 years .The prescribed limits are not strictly respected but results are encouraging and the margin of improvement is large. Considering the activity response, showed in figure 41, after 100 years the reduction between any of the tested V-Cr-Ti-Ta-W alloy and the Inconel is about 6 order of magnitude; the best performances are again attributable to the alloy G after 100 years and to alloy C on a longer period. Anyway, the main difference is between Inconel and HEA in general, while the behaviour of single different composition is secondary.

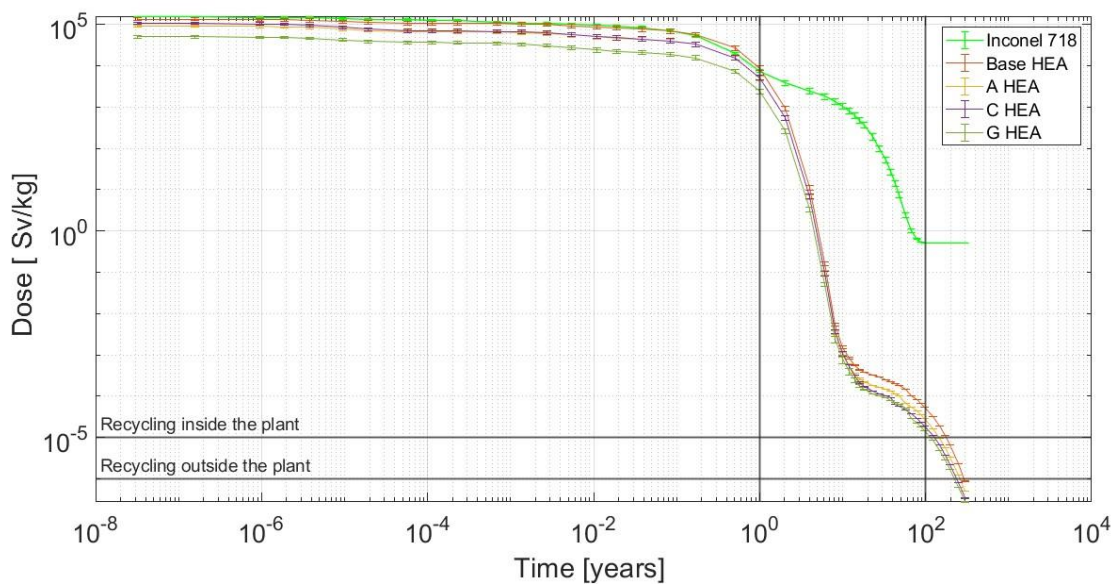


Figure 39 Inconel 718 vs High Entropy Alloys: specific dose

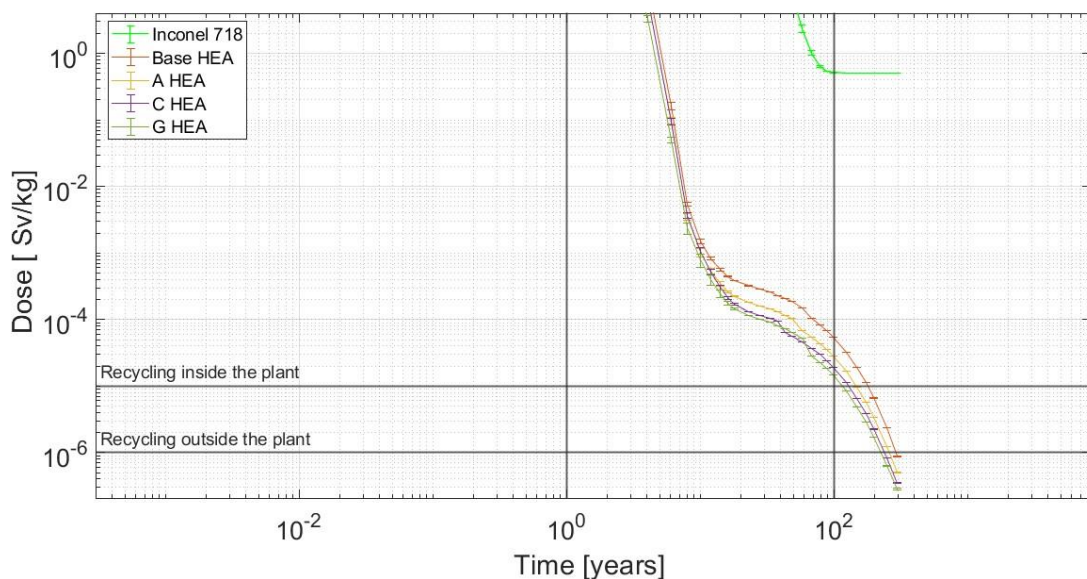


Figure 40 Inconel 718 vs High Entropy Alloys: specific dose, focus

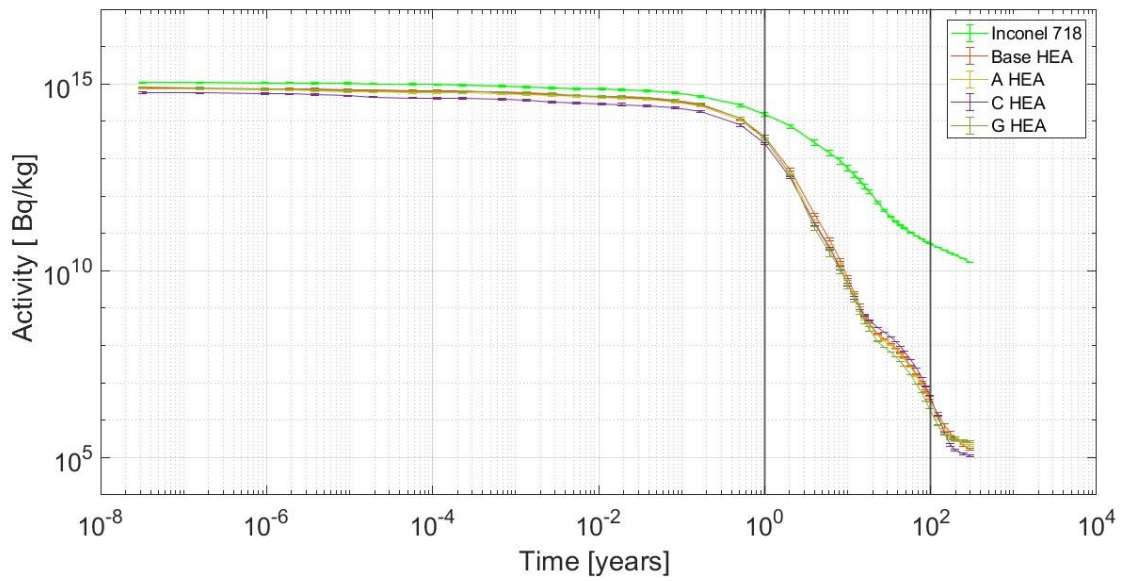


Figure 41 Inconel 718 vs High Entropy Alloys: specific activity

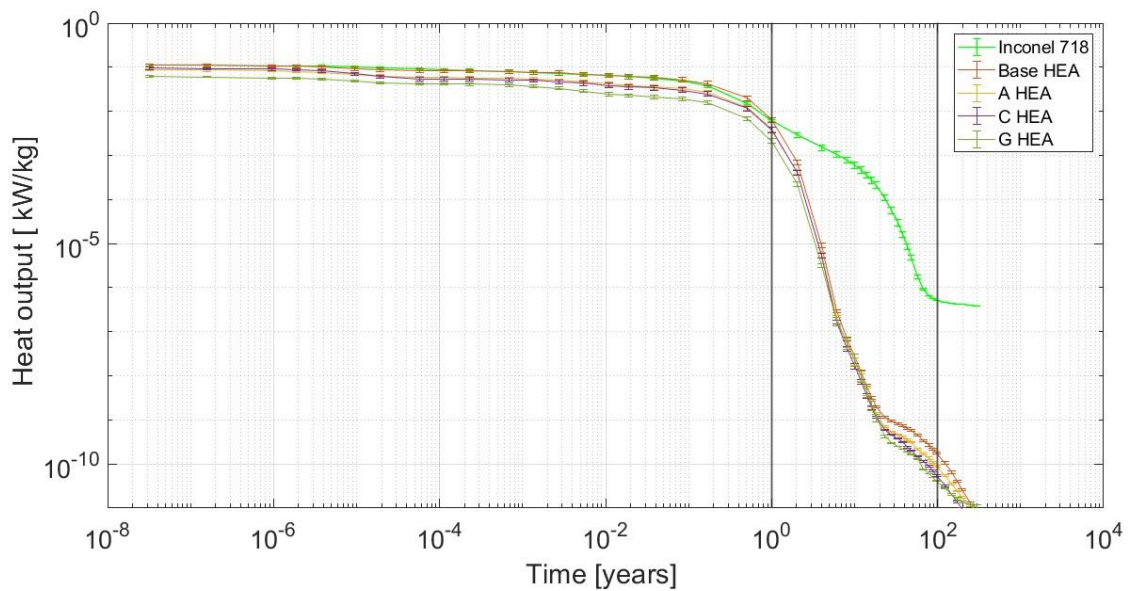


Figure 42 Inconel 718 vs High Entropy Alloys: specific heat output

A strong reduction to the specific heat output, as shown in fig. 42, is clearly associated with the reduced activity of HEA; this aspect can sensibly simplify the management of wastes during the repository time, waiting for recycling, with a general reduction of cost.

### **3.3 IMPURITY ANALYSIS**

Impurities in metallic alloys are inevitable and they can modify consistently the predicted behaviour of materials, with dramatic results for what concern activation and radioactivity. The presence of a small fraction of heavy nuclei, like U, could induce a strong response in structural materials; clearly in the nuclear field alloys should be produced as pure as possible but it can induce a strong increase of costs. From an economic perspective, verify which are the tolerable fractions of impurities still allowing the achievement of the prescribed goals can be fundamental; consequently, in the following section impurities will be added to the tested HEA and simulations will be performed, comparing the results with the Inconel 718 performances. The last chapter of activation section is devoted to a sensitivity analysis on the alloy G, which is associated with the highest TBR; impurity concentration will be multiplied by 10, 100 and 1000, simulating the effect on the goal achievement.

### **3.3.1 ACTIVATION ANALYSIS IN PRESENCE OF IMPURITIES**

The analysis provided in cp. 3.2 has been repeated in the present section for alloys base, A, C and G, including the most probable impurities; since a specific literature for analysed HEA impurities is not available, impurities for W, Ta and V-Cr-Ti individually considered were used. For V-Cr-Ti the impurities presented in [22] was considered; to obtain the correct fraction of each of 3 main elements in the alloy these impurities have been summed up and then the result, divided by 3, was subtracted to V, Cr and Ti concentration respectively. This approach corresponds to consider a uniform distribution for impurities in the 3 elements. Impurities for W and Ta was obtained respectively from [24] and [25]; W impurities are referred to a material obtained by sintering of tungsten powder with purity of 99.999% (5N-W), while Ta impurities were isolated in a tantalum matrix extracted from aqueous solutions containing hydrofluoric and hydrochloric acid into methyl isobutyl ketone. The study presented results for 2 samples, impurities in the present work are referred to sample 2. The impurities for each of the 3 main component of the alloy, (Ta, Cr-Ti-V and W) are listed in tab 9,10,11, with their abundance in ppm and percentage fraction on the element. In table 12 the total impurity composition of the HEA is listed, with percentual fraction on each alloy; fractions of the same element present more than once were summed up (e.g., Ni can be found both in V-Cr-Ti and in Ta; the total Ni impurity is obtained summing up the two fraction). The main elements fractions of the alloy after impurities subtraction are presented in table 13.

table 9 V-Cr-Ti impurities [20]

<b>impurity</b>	<b>ppm on the element</b>	<b>% on the element</b>
Cd	0.05	0.000005
N	0.1	0.00001
O	0.2	0.00002
Al	0.1	0.00001
Si	0.3	0.00003
Fe	0.1	0.00001
Ni	0.01	0.000001
Cu	0.005	0.0000005
Nb	0.001	0.0000001
Mo	0.025	0.0000025
Te	0.05	0.000005

table 10 W impurities [22]

<b>impurity</b>	<b>ppm on the element</b>	<b>% on the element</b>
O	5	0.0005
N	5	0.0005
C	5	0.0005
Na	0.1	0.00001
K	0.05	0.000005
Al	0.05	0.000005
Ca	0.2	0.00002
Cu	0.05	0.000005
Fe	15	0.0015

table 11 Ta impurities [23]

<b>impurity</b>	<b>ppm on the element</b>	<b>% on the element</b>
Pb	0.14	0,000014
Th	0.11	0.000011
U	0.17	0.000017
Al	2.15	0.000215
Mn	0.12	0.000012
Co	0.72	0.000072
Ni	8.35	0.000835
Cu	0.35	0.000035
Zn	0.32	0.000032
Sr	0.07	0.000007
Zr	29.3	0.00293
Nb	18.3	0.00183
Mo	4.2	0.00042
Ag	0.52	0.000052
Cd	0.1	0.00001
Ba	0.11	0.000011
Hf	0.5	0.00005

table 12 total impurities percentual fraction on each alloy

IMPURITY	Base	A	C	G
Pb	0.0000028	0.0000014	0.0000014	0.0000007
Th	0.0000022	0.0000011	0.0000011	0.00000055
U	0.0000034	0.0000017	0.0000017	0.00000085
Al	0.00005	0.0000285	0.0000295	0.00001675
Mn	0.0000024	0.0000012	0.0000012	0.0000006
Co	0.0000144	0.0000072	0.0000072	0.0000036
Ni	0.0001676	0.000084	0.0000842	0.000042
Cu	0.0000083	0.00000575	0.00000485	5.375E-06
Zn	0.0000064	0.0000032	0.0000032	0.0000016
Sr	0.0000014	0.0000007	0.0000007	0.00000035
Zr	0.000586	0.000293	0.000293	0.0001465
Nb	0.00036606	0.00018305	0.00018307	9.1525E-05
Mo	0.0000855	0.00004325	0.00004375	2.1625E-05
Ag	0.0000104	0.0000052	0.0000052	0.0000026
Cd	0.000005	0.0000035	0.0000045	0.00000175
Ba	0.0000022	0.0000011	0.0000011	0.00000055
Hf	0.00001	0.000005	0.000005	0.0000025
O	0.000112	0.00021	0.000114	0.000355
N	0.000106	0.000205	0.000107	0.0003525
C	0.0001	0.0002	0.0001	0.00035
Na	0.000002	0.000004	0.000002	0.000007
K	0.000001	0.000002	0.000001	0.0000035
Ca	0.000004	0.000008	0.000004	0.000014
Fe	0.000306	0.000605	0.000307	0.0010525
Si	0.000018	0.000015	0.000021	0.0000075
Te	0.000003	0.0000025	0.0000035	0.00000125

table 13 main element composition for tested alloys

ALLOY	base	A	C	G
V	19.9999812	29.9999843	59.999978	19.9999922
CR	19.9999812	9.99998432	4.99997804	2.49999216
W	19.999391	39.998782	19.999391	69.9978685
TA	19.9986894	9.9993447	9.9993447	4.99967235
TI	19.9999812	9.99998432	4.99997804	2.49999216

To verify the impact of impurities on the performances, the 4 HEA have been compared with Inconel 718, in figure 43,44,45.

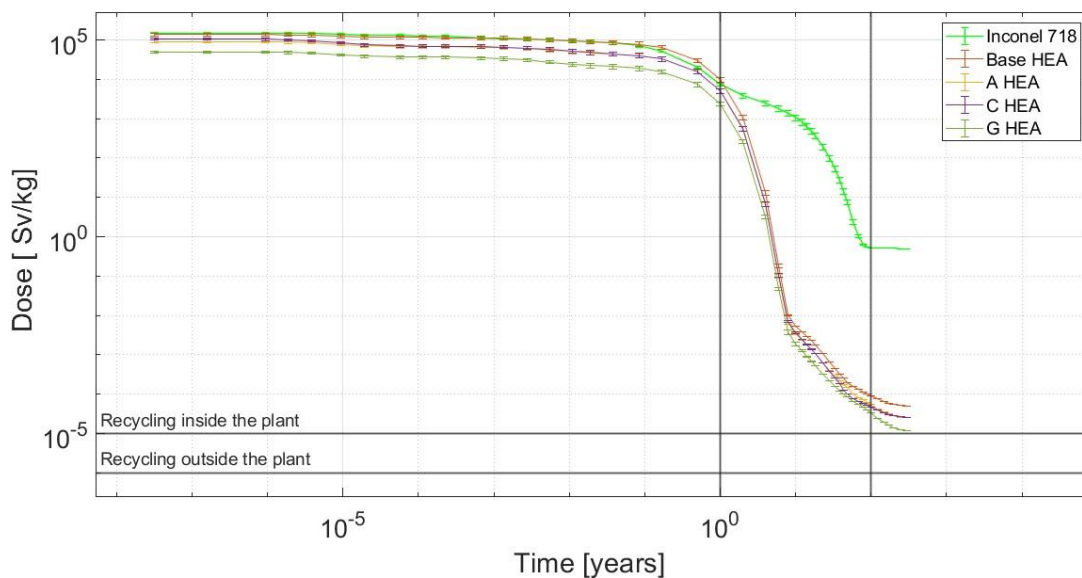


Figure 43 Inconel 718 vs High Entropy Alloys with impurities: specific dose

The presence of traces of nuclides other than V-Cr-Ti-Ta-W causes a depletion of performances, at the point that in plant recycling requires at least 290 years, disregarding the proposed limit; anyway, a reduction on dose of 4 order of magnitude with respect to Inconel 718 is still obtained. Alloy G seems to be the less damaged from impurity presence. It can be due to the small contamination in Ni, the smallest in absolute; Ni is known as the most responsible nuclide for high activation in Inconel 718. Similar considerations are valid for activity and heat output results, showed in figures 44 and 45; despite the reduction of performances the main difference remains between the Inconel 718 and HEA, with similar behaviour for all the tested composition. Also in this frame alloy G is confirmed

as the best performing, probably thanks to its reduced Ni fraction; the difference between alloy G and base, A and C, anyway, is less pronounced for what concern activity and heat output.

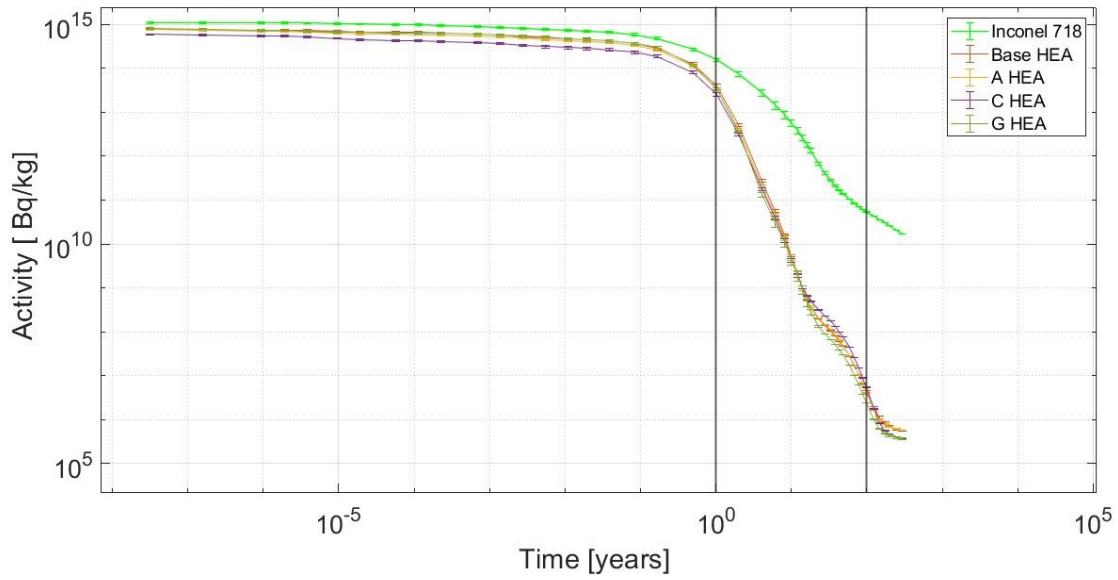


Figure 44 Inconel 718 vs High Entropy Alloys with impurities: specific activity

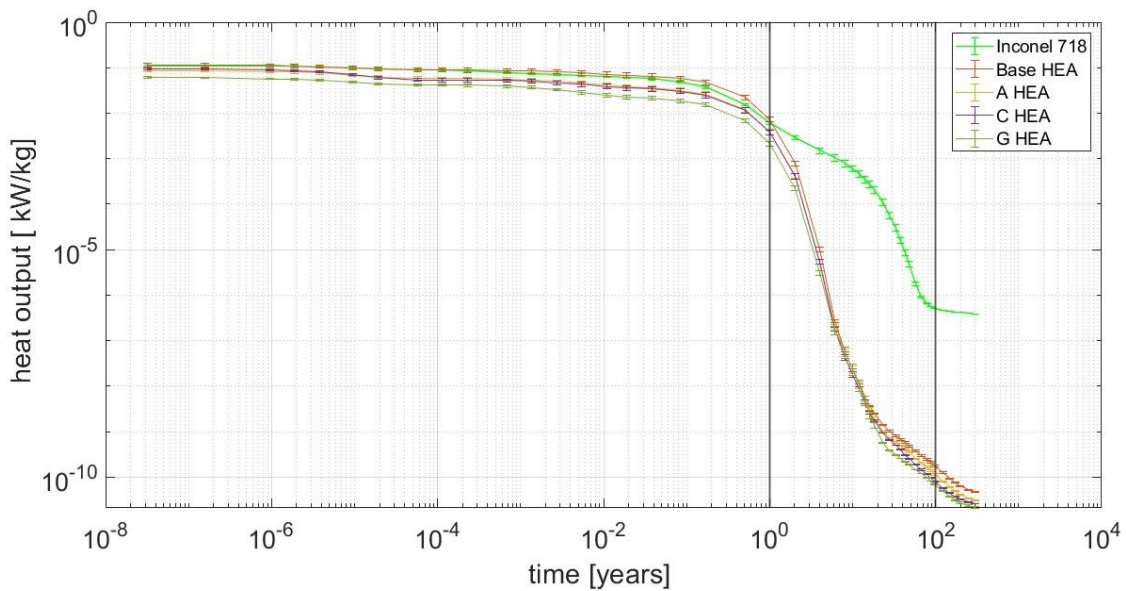


Figure 45 Inconel 718 vs High Entropy Alloys with impurities: specific heat output

The worst performance is scored by base alloy for all the 3 aspects; it contains the highest Ni contamination, one order of magnitude more than alloy G and this strengthens the hypothesis that it is primarily responsible for low activation resistance. In general, also considering impurities, HEA alloys are able to overperform consistently Inconel 718; a reduction of 4 order of magnitude is still possible in terms of both specific activity and heat output. Alloy G seems to be the most interesting configuration for both TBR and activation result; it is interesting to compare directly the case with and without impurities for this alloy, to state the differences. For what concern the dose, the curves are basically coincident for the first 10 years, when they start to diverge; a focus on this period is proposed in figure 46.

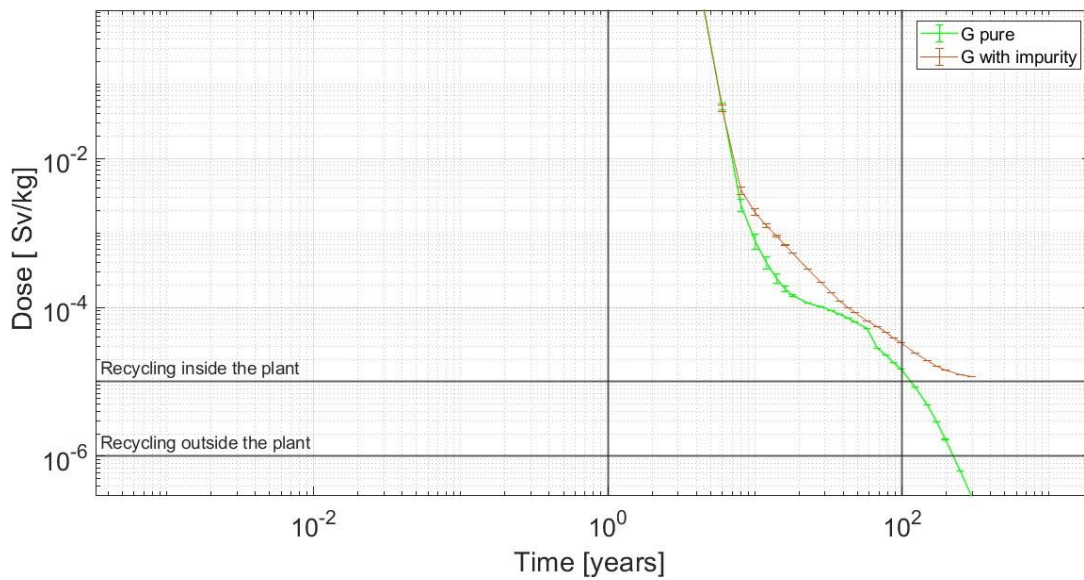


Figure 46 High Entropy Alloy G pure vs with impurities: specific dose, focus

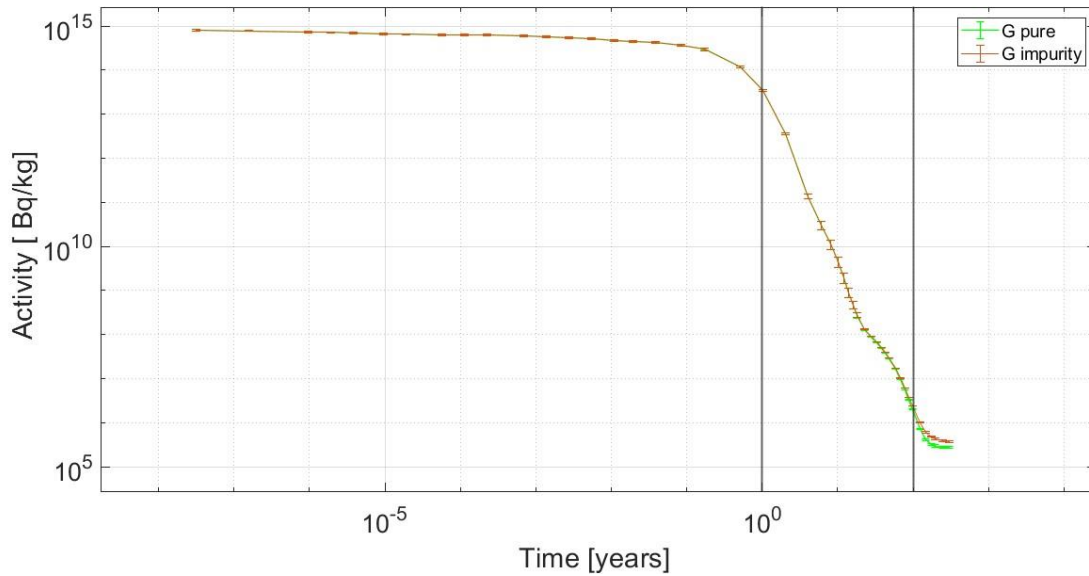


Figure 47 High Entropy Alloy G pure vs with impurities: specific activity

The difference is not dramatic for the first 10 years, when the curves start to diverge; the outplant recycling appears to be complex for the alloy with impurities, which converges slowly to  $10E-5$  Sv/kg; conversely the pure alloy demonstrates a much faster decay in the specific dose, with a difference of 2 order of magnitude in around 200 years. The described trend of performances reduction appears to be quite general, since it can be individuated also for specific activity and heat output results; Qualitatively, a depletion of one order of magnitude after 130 years can be assessed as consequence of impurities.

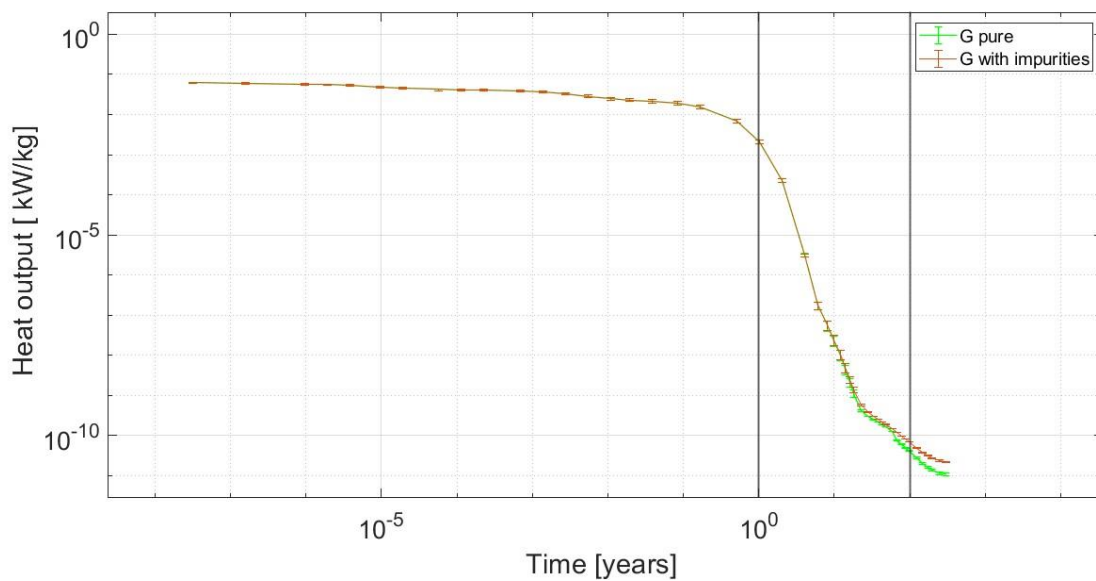


Figure 48 High Entropy Alloy G pure vs with impurities : specific heat output

### 3.3.2 SENSITIVITY ANALYSIS

As shown in chap. 3.3.1 the presence of impurities has a strong impact on the activation performances of alloys. To evaluate it more precisely, a sensitivity analysis has been conducted on alloy G, the most interesting and impurity-resistant, multiplying the impurity fraction time 10, 100 and 1000 (calling the obtained alloys C1, C2, C3 and C4); the results were compared with the pure alloy and with Inconel 718, to state if also in unrealistic cases the HEA are able to maintain their superiority. Clearly, increasing the fraction of unwilled nuclides, the percentage of V, Cr, Ti, Ta and W in the material decreases; in table 14 the resulting compositions are listed. The precise quantities of impurities, conversely, are listed in table 15.

*table 14 High Entropy Alloy main elements fraction associated to different impurities fractions*

<b>Impurity</b>	<b>C1 (x1)</b>	<b>C2 (x10)</b>	<b>C3 (x100)</b>	<b>C4 (x1000)</b>
V	19.9999922	19.9999216	19.9992158	19.9921583
CR	2.49999216	2.49992158	2.49921583	2.49215833
W	69.9978685	69.978685	69.78685	67.8685
TA	4.99967235	4.9967235	4.967235	4.67235
TI	2.49999216	2.49992158	2.49921583	2.49215833

In figure 49 the dose output is reported; the analysis involves 3 order of magnitude for impurities variation, so the performance depletion is quite consistent between the “pure case “and C4 , with an increment of at least 4 order of magnitude in the specific dose. Also this last case, despite it appears as very unrealistic, overperforms Inconel 718, allowing a reduction of 2 order of magnitude in the dose after 1 century. The “in plant “recycling goal appears to be achieved for the pure alloy, achievable with reserve for C1 alloy, while C2, C3 and C4 are not able to satisfy the proposed limits for low activation materials in the first 300 years; still, they can constitute an interesting improvement with respect to more classical materials and the huge amount of impurities contained in can moderate sensibly their production cost; for these reasons C3 and C4 could be considered as “reduced activation materials”.

The results for specific heat output and activity are presented in figures 50 and 51; the behaviour described for what concern the dose is repeated also in these cases, so that the higher the impurities, the higher the output after a century of decay. Qualitatively, increasing of 3 order of magnitude the impurity fraction, a depletion of 3-4 order of magnitude is caused on the result after a century; anyway, HEA can consistently overperform Inconel 718 also for heat output and activity.

table 15 impurities and concentration applied to the sensitivity analysis

IMPURITY	x1	x10	x100	x1000
Pb	0.0000007	0.000007	0.00007	0.0007
Th	0.00000055	0.0000055	0.000055	0.00055
U	0.00000085	0.0000085	0.000085	0.00085
Al	0.00001675	0.0001675	0.001675	0.01675
Mn	0.0000006	0.000006	0.00006	0.0006
Co	0.0000036	0.000036	0.00036	0.0036
Ni	0.000042	0.00042	0.0042	0.042
Cu	5.375E-06	0.00005375	0.0005375	0.005375
Zn	0.0000016	0.000016	0.00016	0.0016
Sr	0.00000035	0.0000035	0.000035	0.00035
Zr	0.0001465	0.001465	0.01465	0.1465
Nb	9.1525E-05	0.00091525	0.0091525	0.091525
Mo	2.1625E-05	0.00021625	0.0021625	0.021625
Ag	0.0000026	0.000026	0.00026	0.0026
Cd	0.00000175	0.0000175	0.000175	0.00175
Ba	0.00000055	0.0000055	0.000055	0.00055
Hf	0.0000025	0.000025	0.00025	0.0025
O	0.000355	0.00355	0.0355	0.355
N	0.0003525	0.003525	0.03525	0.3525
C	0.00035	0.0035	0.035	0.35
Na	0.000007	0.00007	0.0007	0.007
K	0.0000035	0.000035	0.00035	0.0035
Ca	0.000014	0.00014	0.0014	0.014
Fe	0.0010525	0.010525	0.10525	1.0525
Si	0.0000075	0.000075	0.00075	0.0075
Te	0.00000125	0.0000125	0.000125	0.00125

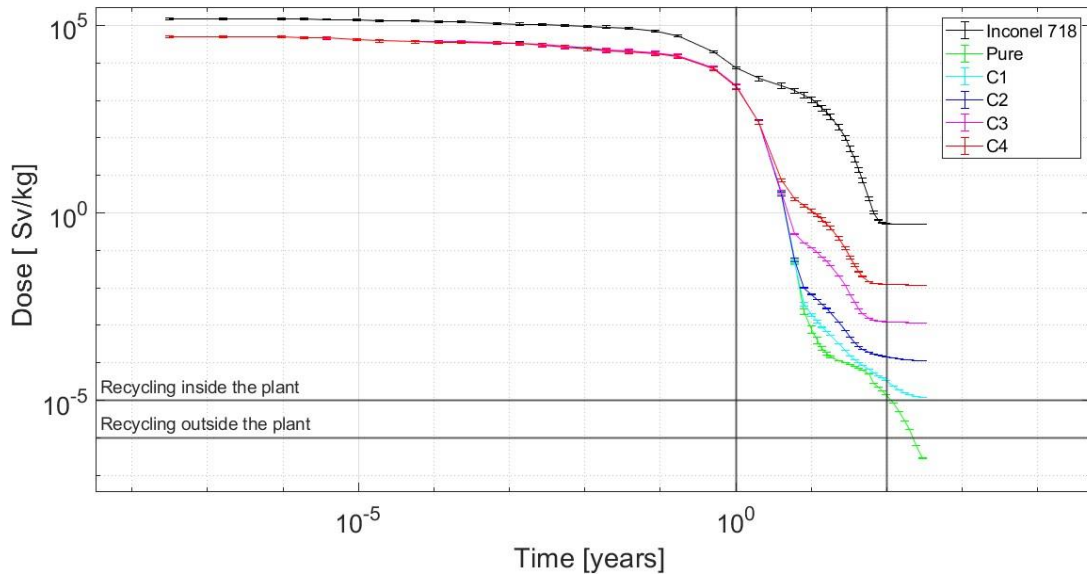


Figure 49 sensitivity analysis on impurities: specific dose

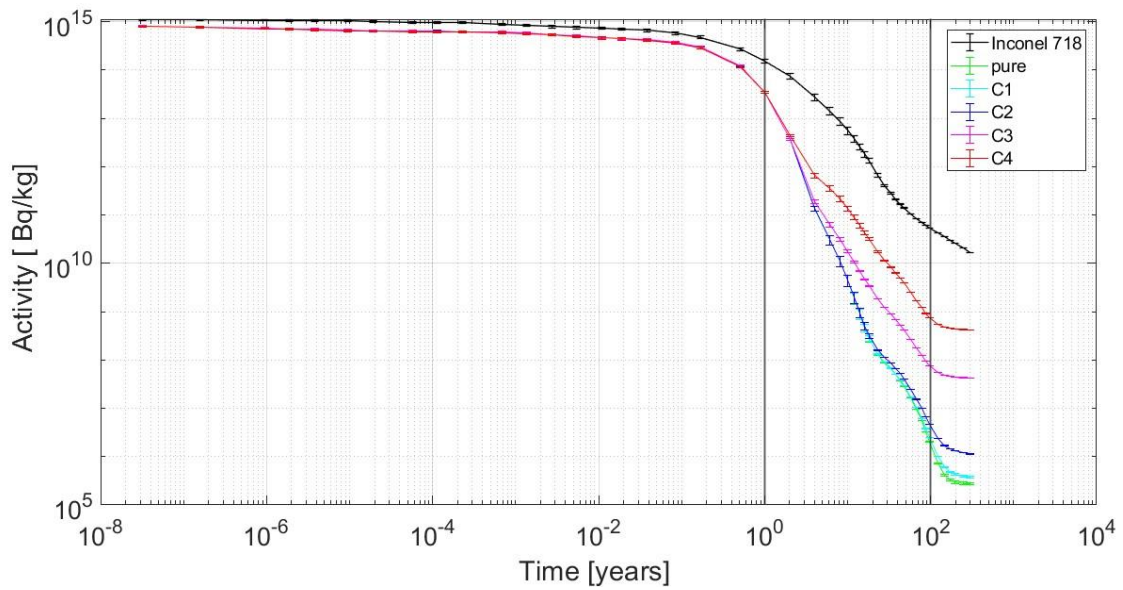


Figure 50 sensitivity analysis on impurities: specific activity

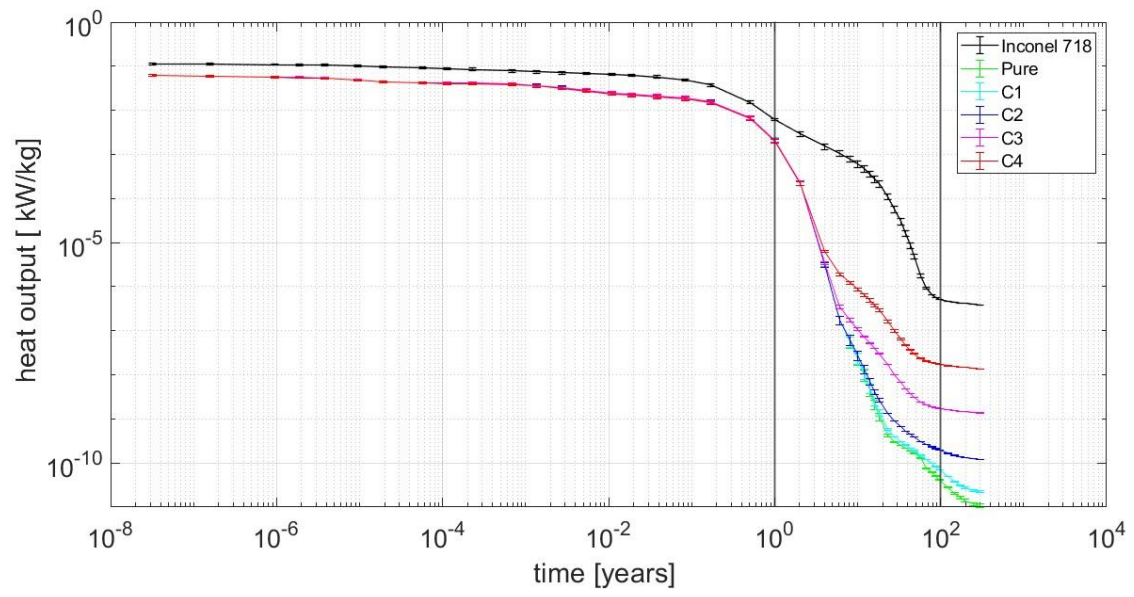


Figure 51 sensitivity analysis on impurities: specific heat output

## 4 CONCLUSIONS

V-Cr-Ti-Ta-W high entropy alloys demonstrate their superiority on Inconel 718 under both the investigated field of tritium breeding capability and activation issue. All the proposed compositions, from the basic equimolar to the W based alloy are able to provide a TBR larger than 1.1 without any solid neutron multiplier layer, a result which was demonstrated as non-possible with Inconel 718. The goal of eliminating the solid Beryllium from the layout is satisfied and a large enough margin is guaranteed to balance inevitable leakages during the tritium extraction and production. High presence of W seems to be associated with higher breeding performances and a further analysis on costs should be carried out, testing different levels of W-184 enrichment. The mechanical properties of the proposed alloys, furthermore, have not been investigated; due to the hard conditions inside the reactor they are still fundamental, and a study should be conducted also in this direction. The limit proposed for “in plant” recycling in one century is strictly not satisfied by any of the proposed HEA, with a worsening in presence of impurities at the concentration mentioned in the available literature; alloy G is able to reach the “in-plant recycling” in around 120 years, if produced pure. Anyway, the Inconel 718 is consistently overperformed and V-Cr-Ti-Ta-W alloy can be considered at least as “reduced activation material”. The presence of impurities can deplete performances consistently only if concentrations up to 2 orders of magnitude over nominal are reached; also in this case the usage of HEA allows a consistent reduction of activity, heat output and dose with respect to Inconel 718 after 100 years. The G composition is confirmed as the best candidate also in this frame, probably due to its low fraction of Ni, considered as the main responsible for Inconel 718 bad behaviour.

## Bibliography

- [1] Freidberg, J., "Plasma physics and Fusion Energy", New York, USA, Cambridge University Press
- [2] <https://en.wikipedia.org/wiki/Tritium>
- [3] [https://www.wikiwand.com/it/Fusione\\_nucleare](https://www.wikiwand.com/it/Fusione_nucleare)
- [4] <http://www.fusione.enea.it/WHAT/fusion1.html.en>
- [5] <https://it.wikipedia.org/wiki/Tokamak>
- [6] Kovari M. et al., Nucl. Fus. 58:026010, 2018
- [7] prof. Zanino R., 2020-2021, Slides of the course "Nuclear Fusion reactor engineering"
- [8] <https://en.wikipedia.org/wiki/Lithium>
- [9] B.N. Sorbom, et al., «ARC: A compact, high-field, fusion nuclear science facility and demonstration power plant with demountable magnets,» *Fusion Engineering and Design*, vol. 100, pp. 378-405, 2015.
- [10] <https://en.wikipedia.org/wiki/Lithium>
- [11] Ming-Hung Tsai et al., "high entropy alloys: a critical review", *Material Research Letters*, vol.2, pp. 107-123, 2014
- [12] <https://it.wikipedia.org/wiki/ITER>
- [13] A. Q. Kuang, et al., "Conceptual design study for heat exhaust management in the ARC fusion", *Fusion Engineering and Design*, vol. 137, pp. 221-242, 2018.
- [14] Owais Ahmed Waseem et al., "Powder Metallurgy Processing of a  $W_x$ -Ta-Ti-V-Cr High-Entropy Alloy and Its Derivative Alloys for Fusion Material Applications", *Scientific Reports*, vol.7, art. n. 1926, 2017
- [15] Sobieraj D. et al., "Chemical short-range order in derivative Cr-Ta-Ti-V-W high entropy alloys from the first-principles thermodynamic study", *Physical Chemistry Chemical Physics*, 2020
- [16] <https://docs.openmc.org/en/stable/usersguide/index.html>
- [17] S. Segantin, et al., "Optimization of tritium breeding ratio in ARC reactor", *Fusion Engineering and Design*, vol. 154, n. 111531, 2020.
- [18] <https://pypi.org/project/openmc-plasma-source/>
- [19] [http://www.specialmetals.com/assets/smc/documents/inconel\\_alloy\\_718.pdf](http://www.specialmetals.com/assets/smc/documents/inconel_alloy_718.pdf),
- [20] S. Segantin, et al., "ARC reactor – Neutron irradiation analysis", *Fusion Engineering and Design*, vol. 159, n. 111792, 2020.
- [21] M. Fleming et al., "The FISPACT-II user manual", UKAEA-R(18)001 Issue , February 2018

- [22] S. Fukuzumi et al., “Defect structural evolution in high purity tungsten irradiated with electrons using high voltage electron microscope”, *Journal of Nuclear Materials* vol. 343, Issues 1–3, pp. 308-312, 1 August 2005,
- [23] Vijay K.Panday et al., “Determination of trace impurities in tantalum by inductively coupled plasma mass spectrometry after removal of the matrix by liquid-liquid extraction”, *Analytica Chimica Acta*, vol. 329, Issues 1–2, pp. 153-159, , 9 August 1996

# List of figures

FIGURE 1 FUSION REACTION RATE AS FUNCTION OF T [3] .....	7
FIGURE 2 DEUTERIUM-TRITIUM FUSION REACTION [4] .....	8
FIGURE 3 EXAMPLE OF A TOKAMAK MACHINE [5] .....	9
FIGURE 4 TOKAMAK MAGNETIC FIELDS AND COILS [5].....	10
FIGURE 5 MAGNETIC FIELD GENERATION .....	<b>ERROR! BOOKMARK NOT DEFINED.</b>
FIGURE 6 MAGNETIC FIELD COMPONENTS AND THEIR GENERATION [5] .....	<b>ERROR! BOOKMARK NOT DEFINED.</b>
FIGURE 7 TRITIUM INVENTORY EVOLUTION SCENARIOS [6].....	11
FIGURE 8 $\text{Li-6}(n,\alpha)\text{T}$ AND $\text{Li-7}(n,n,\alpha)\text{T}$ CROSS-SECTION [7].....	12
FIGURE 9 STRUCTURE MODEL OF A $\text{CoCrFeMnNi}$ ALLOY [10] .....	13
FIGURE 10 ARC VS MAN SIZE COMPARISON [8] .....	15
FIGURE 11A PICTURE OF DEMOUNTABLE TOROIDAL COILS [8].....	16
FIGURE 12 ARC MAIN PARAMETERS [8] .....	16
FIGURE 13 ITER MAIN PARAMETERS [14].....	16
FIGURE 14 FLiBe TANK SURROUNDING THE VACUUM VESSEL [8] .....	17
FIGURE 15 REPRESENTATION OF VACUUM VESSEL STRUCTURE [15] .....	18
FIGURE 16 D MODEL CROSS SECTION AND PARTICULAR .....	21
FIGURE 17 TOKAMAK SOURCE NEUTRON DENSITY .....	24
FIGURE 18 CROSS SECTION OF THE SOURCE LOCATED INSIDE THE D MODEL: ION TEMPERATURE REPRESENTATION .....	24
FIGURE 19 TOKAMAK SOURCE NEUTRON DENSITY PROFILE .....	25
FIGURE 20 TOKAMAK SOURCE ION TEMPERATURE PROFILE .....	25
FIGURE 22 FLUX DISTRIBUTION, Be LAYER, INCONEL 718.....	28
FIGURE 21 LUX DISTRIBUTION, NO Be LAYER, INCONEL 718.....	28
FIGURE 24 TBR MEAN VALUE, Be LAYER, INCONEL 718 .....	28
FIGURE 23 TBR MEAN VALUE, NO Be LAYER, INCONEL 718.....	28
FIGURE 25 STANDARD DEVIATION, NO Be, INCONEL 718 .....	29
FIGURE 26 STANDARD DEVIATION, Be LAYER, INCONEL 718 .....	29
FIGURE 27 TOTAL TBR WITH AND WITHOUT BERYLLIUM LAYER .....	29
FIGURE 28 FRACTION OF TRITIUM PRODUCTION IN THE CHANNEL AND IN THE TANK .....	30
FIGURE 29 TBR OBTAINED WITH 8 DIFFERENT HIGH ENTROPY ALLOYS .....	31
FIGURE 30 TBR AS FUNCTION OF ALLOY DENSITY .....	32
FIGURE 31 TBR AS FUNCTION OF V FRACTION.....	33
FIGURE 32 TBR AS FUNCTION OF Cr FRACTION .....	34
FIGURE 33 TBR AS FUNCTION OF W FRACTION .....	34
FIGURE 34 TBR AS FUNCTION OF Ta FRACTION .....	35
FIGURE 35 TBR AS FUNCTION OF Ti FRACTION .....	35
FIGURE 36 FLUX DISTRIBUTION , HIGH ENTROPY ALLOY G .....	36
FIGURE 37 TBR STANDARD DEVIATION, HIGH ENTROPY ALLOY G .....	36
FIGURE 38 TBR DISTRIBUTION, HIGH ENTROPY ALLOY G .....	36
FIGURE 39 NEUTRON FLUX NORMALIZED ON THE SOURCE.....	39
FIGURE 40 INCONEL 718 VS HIGH ENTROPY ALLOYS: SPECIFIC DOSE.....	40
FIGURE 41 INCONEL 718 VS HIGH ENTROPY ALLOYS: SPECIFIC DOSE, FOCUS.....	40
FIGURE 42 INCONEL 718 VS HIGH ENTROPY ALLOYS: SPECIFIC ACTIVITY .....	41
FIGURE 43 INCONEL 718 VS HIGH ENTROPY ALLOYS: SPECIFIC HEAT OUTPUT.....	41
FIGURE 44 INCONEL 718 VS HIGH ENTROPY ALLOYS WITH IMPURITIES: SPECIFIC DOSE .....	47
FIGURE 45 INCONEL 718 VS HIGH ENTROPY ALLOYS WITH IMPURITIES: SPECIFIC ACTIVITY .....	48
FIGURE 46 INCONEL 718 VS HIGH ENTROPY ALLOYS WITH IMPURITIES: SPECIFIC HEAT OUTPUT .....	48
FIGURE 47 HIGH ENTROPY ALLOY G PURE VS WITH IMPURITIES : SPECIFIC DOSE, FOCUS.....	49
FIGURE 48 HIGH ENTROPY ALLOY G PURE VS WITH IMPURITIES : SPECIFIC ACTIVITY .....	50
FIGURE 49 HIGH ENTROPY ALLOY G PURE VS WITH IMPURITIES : SPECIFIC HEAT OUTPUT .....	50
FIGURE 50 SENSITIVITY ANALYSIS ON IMPURITIES: SPECIFIC DOSE .....	53

FIGURE 51 SENSITIVITY ANALYSIS ON IMPURITIES: SPECIFIC ACTIVITY.....	53
FIGURE 52 SENSITIVITY ANALYSIS ON IMPURITIES: SPECIFIC HEAT OUTPUT .....	54

# List of tables

TABLE 1 THICKNESSES OF EACH LAYER .....	22
TABLE 2 SOURCE SET PARAMETERS [8] .....	23
TABLE 3 INCONEL 718 COMPOSITION, % IN MASS [20].....	26
TABLE 4 HIGH ENTROPY ALLOYS COMPOSITIONS .....	27
TABLE 5 TBR AND STANDARD DEVIATIONS; INCONEL 718 AS STRUCTURAL MATERIAL.....	30
TABLE 6 PRECISE T PRODUCTION FRACTION IN EACH LAYER .....	30
TABLE 7 HIGH ENTROPY ALLOYS WITH RELATIVE TBR AND STANDARD DEVIATION .....	32
TABLE 8 RECYCLING LIMITS .....	37
TABLE 9 V-CR-Ti IMPURITIES [20] .....	44
TABLE 10 W IMPURITIES [22] .....	44
TABLE 11 TA IMPURITIES [23] .....	45
TABLE 12 TOTAL IMPURITIES PERCENTUAL FRACTION ON EACH ALLOY .....	46
TABLE 13 MAIN ELEMENT COMPOSITION FOR TESTED ALLOYS .....	47
TABLE 14 HIGH ENTROPY ALLOY MAIN ELEMENTS FRACTION ASSOCIATED TO DIFFERENT IMPURITIES FRACTIONS .....	51
TABLE 15 IMPURITIES AND CONCENTRATION APPLIED TO THE SENSITIVITY ANALYSIS .....	52

# Appendix A

Example of OpenMC script: D-shape model with high-entropy alloy.

```
import openmc

import matplotlib.pyplot as plt

from openmc_plasma_source import TokamakSource, plot_tokamak_source_3D,
scatter_tokamak_source

from plotly.offline import download_plotlyjs, plot

from plotly.graph_objs import Scatter, Layout

#####

# Create materials for the problem

w = openmc.Material(name='Tungsten') #first wall
w.add_nuclide('W184', 1.)
w.set_density('g/cm3', 19.250)
w.temperature = 900.0 # temperature in Kelvin

hea = openmc.Material(name='High-entropy alloy HEA') #structural layers
hea.add_element('V', 0.2,'wo')
hea.add_element('Cr', 0.2,'wo')
hea.add_element('W', 0.2,'wo')
hea.add_element('Ta', 0.2,'wo')
hea.add_element('Ti', 0.2,'wo')
hea.set_density('g/cm3', 10.7314)
hea.temperature = 900.0

flibe = openmc.Material(name='FLiBe') #breeding blanket (Li-6 enrichment 90 %)
flibe.add_element('F', 4.)
flibe.add_element('Be', 1.)
flibe.add_nuclide('Li6', 1.8)
```

```

flibe.add_nuclide('Li7', 0.2)
flibe.set_density('g/cm3', 1.94)
flibe.temperature = 900.0

be = openmc.Material(name='Berillium') #neutron multiplier
be.add_element('Be', 1.)
be.set_density('g/cm3', 1.848)
be.temperature = 900.0

void = openmc.Material(name='Void') #hydrogen to simulate vacuum
void.add_element('H', 1.0)
void.set_density('g/cm3', 0.0001)
void.temperature = 900.0

wc = openmc.Material(name='Tungsten Carbide')
wc.add_element('C', 1.)
wc.add_element('W', 1.)
wc.set_density('g/cm3', 15.63)
wc.temperature = 900.0

# Collect the materials together and export to XML
materials = openmc.Materials([w, hea, flibe, be, void, wc])
materials.export_to_xml()

#####

# GEOMETRY

# high field side planes
hf_fw_inner = openmc.XPlane(x0=-42.9+330-50, name='hf fw inner')

```

```

hf_str1_inner = openmc.XPlane(x0=-43.0+330-50, name='hf str1 inner')
hf_channel_inner = openmc.XPlane(x0=-44.0+330-50, name='hf channel inner')
hf_nmult_inner = openmc.XPlane(x0=-46.0+330-50, name='hf nmult inner')
hf_str2_inner = openmc.XPlane(x0=-47.0+330-50, name='hf str2 inner')
hf_blanket_inner = openmc.XPlane(x0=-50.0+330-50, name='hf blanket inner')
hf_shield_inner = openmc.XPlane(x0=-100.0+330-50, boundary_type='vacuum',
                                name='hf shield inner')
#hf_shield_outer = openmc.XPlane(x0=-120.0+330-50, boundary_type='vacuum',
                                name="hf shield outer")

# low field side cylinders
lf_fw_inner = openmc.YCylinder(x0=330-50, z0=0, r=139.9, name='lf fw inner')
lf_str1_inner = openmc.YCylinder(x0=330-50, z0=0, r=140.0, name='lf str1 inner')
lf_channel_inner = openmc.YCylinder(x0=330-50, z0=0, r=141.0, name='lf channel inner')
lf_nmult_inner = openmc.YCylinder(x0=330-50, z0=0, r=143.0, name='lf nmult inner')
lf_str2_inner = openmc.YCylinder(x0=330-50, z0=0, r=144.0, name='lf str2 inner')
lf_blanket_inner = openmc.YCylinder(x0=330-50, z0=0, r=147.0, name='lf blanket inner')
lf_shield_inner = openmc.YCylinder(x0=330-50, z0=0, r=197.0, boundary_type='vacuum',
                                   name='lf shield inner')
#lf_shield_outer = openmc.YCylinder(x0=330-50, z0=0, r=217.0, boundary_type='vacuum',
                                   name='lf shield outer')

# Z planes
lower_bound = openmc.YPlane(y0=-50, boundary_type='reflective')
upper_bound = openmc.YPlane(y0=50, boundary_type='reflective')

# selecting regions
PLASMA = +hf_fw_inner & -lf_fw_inner & +lower_bound & -upper_bound
FW = ((-hf_fw_inner & +hf_str1_inner & -lf_str1_inner) |
      (+lf_fw_inner & -lf_str1_inner & +hf_str1_inner)) &
      +lower_bound & -upper_bound

```

```
STR1 = ((-hf_str1_inner & +hf_channel_inner & -lf_channel_inner) |  
        (+lf_str1_inner & -lf_channel_inner & +hf_channel_inner)) &  
        +lower_bound & -upper_bound
```

```
CHANNEL = ((-hf_channel_inner & +hf_nmult_inner & -lf_nmult_inner) |  
           (+lf_channel_inner & -lf_nmult_inner & +hf_nmult_inner)) &  
           +lower_bound & -upper_bound
```

```
NMULT = ((-hf_nmult_inner & +hf_str2_inner & -lf_str2_inner) |  
         (+lf_nmult_inner & -lf_str2_inner & +hf_str2_inner)) &  
         +lower_bound & -upper_bound
```

```
STR2 = ((-hf_str2_inner & +hf_blanket_inner & -lf_blanket_inner) |  
        (+lf_str2_inner & -lf_blanket_inner & +hf_blanket_inner)) &  
        +lower_bound & -upper_bound
```

```
BLANKET = ((-hf_blanket_inner & +hf_shield_inner & -lf_shield_inner) |  
           (+lf_blanket_inner & -lf_shield_inner & +hf_shield_inner)) &  
           +lower_bound & -upper_bound
```

```
#SHIELD = ((-hf_shield_inner & +hf_shield_outer & -lf_shield_outer) |  
          (+lf_shield_inner & -lf_shield_outer & +hf_shield_outer)) &  
          +lower_bound & -upper_bound
```

```
# creating cells
```

```
plasma = openmc.Cell(1, fill=void, name='plasma', region=PLASMA)
```

```
first_wall = openmc.Cell(2, fill=w, name='first wall', region=FW)
```

```
str1 = openmc.Cell(3, fill=hea, name='str1', region=STR1)
```

```
channel = openmc.Cell(4, fill=flibe, name='channel', region=CHANNEL)
```

```
nmult = openmc.Cell(5, fill=be, name='nmult', region=NMULT)
```

```
str2 = openmc.Cell(6, fill=hea, name='str2', region=STR2)
```

```
blanket = openmc.Cell(7, fill=flibe, name='blanket', region=BLANKET)
```

```
#shield = openmc.Cell(8, fill=wc, name='shield', region=SHIELD)
```

```
root_universe = openmc.Universe(cells=(plasma, first_wall, str1, channel, nmult, str2, blanket))
```

```

geometry = openmc.Geometry(root_universe)
geometry.export_to_xml()

#####

#Geometry plotting 2D
plotg = openmc.Plot()
plotg.filename = 'D_model'
plotg.basis = 'xz'
plotg.width = (247*2, 247*2)
plotg.pixels = (400, 400)
plotg.origin = (330, 0, 0)
plotg.color_by = 'material'
plotg.colors = {void: 'white', w: 'red', hea: 'lightslategrey', flibe: 'aqua'}
#plotg.colors = {void: 'white', w: 'red', hea: 'lightslategrey', flibe: 'aqua', wc: 'olive'}
plotg.background = 'black'

plots = openmc.Plots([plotg])
plots.export_to_xml()
openmc.plot_geometry()

#####

# Define problem settings

# Indicate how many particles to run
settings = openmc.Settings()
batches = 30
settings.batches = batches
settings.inactive = 10
settings.particles = 50000
settings.run_mode = 'fixed source'

```

```
# Create an initial source
```

```
my_plasma = TokamakSource(  
    #elongation=1.557,  
    elongation=1.84,  
    #ion_density_centre=1.09e20,  
    ion_density_centre=1.8e20,  
    ion_density_peaking_factor=1,  
    ion_density_pedestal=1.05e20,  
    ion_density_separatrix=1e20,  
    #ion_temperature_centre=45.9,  
    ion_temperature_centre=27,  
    ion_temperature_peaking_factor=8.06,  
    ion_temperature_pedestal=2.5,  
    ion_temperature_separatrix=0.5,  
    major_radius=330,  
    minor_radius=60,  
    pedestal_radius=0.8 * 60,  
    mode="H", # 3 MODES: H, L, A. We use 'H' as suggested in [1]  
    #shafranov_factor=0.44789,  
    shafranov_factor=0.44789,  
    triangularity=0.270,  
    ion_temperature_beta=6  
)
```

```
settings.source = my_plasma.sources
```

```
settings.export_to_xml()
```

```
#####
```

```
# Define tallies

# Instantiate an empty Tallies object
tallies = openmc.Tallies()

# Create mesh which will be used for tally
mesh = openmc.RegularMesh()
mesh.dimension = [500, 1, 500]
mesh.lower_left = [80, -250, -250]
mesh.upper_right = [580, 250, 250]

# Create mesh filter for tally
mesh_filter = openmc.MeshFilter(mesh)

# Create mesh tally to score tritium rate production
cell_filter = openmc.CellFilter([channel.id, nmult.id, blanket.id])
tbr_tally = openmc.Tally(name='TBR')
tbr_tally.filters = [cell_filter]
tbr_tally.scores = ['H3-production']
tallies.append(tbr_tally)

# Create mesh tally to score neutron flux
#cell_filter2 = openmc.CellFilter([fw.id, str1.id, flibe1.id, multiplier.id, str2.id, flibe2.id])
flux_plot_tally = openmc.Tally(name='Flux')
flux_plot_tally.filters = [mesh_filter]
flux_plot_tally.scores = ['flux']
tallies.append(flux_plot_tally)

# Create mesh tally to score tritium rate production in mesh filter to plot Tritium generation
tbrplot_tally = openmc.Tally(name='TBR all values')
tbrplot_tally.filters = [mesh_filter]
```

```
tbrplot_tally.scores = ['H3-production'] #usato al posto di (n,t)
```

```
tallies.append(tbrplot_tally)
```

```
# Create mesh tally to score neutron spectra
```

```
energy_bins = openmc.mgxs.GROUP_STRUCTURES['CCFE-709']
```

```
energy_filter = openmc.EnergyFilter(energy_bins)
```

```
str1_filter = openmc.CellFilter([str1.id])
```

```
str2_filter = openmc.CellFilter([str2.id])
```

```
spectrastr1_tally = openmc.Tally(name='structural_layer_spectra_STR1')
```

```
spectrastr1_tally.filters = [str1_filter, energy_filter]
```

```
spectrastr1_tally.scores = ['flux']
```

```
tallies.append(spectrastr1_tally)
```

```
spectrastr2_tally = openmc.Tally(name='structural_layer_spectra_STR2')
```

```
spectrastr2_tally.filters = [str2_filter, energy_filter]
```

```
spectrastr2_tally.scores = ['flux']
```

```
tallies.append(spectrastr2_tally)
```

```
# Export to "tallies.xml"
```

```
tallies.export_to_xml()
```

```
#####
```

```
# Run OpenMC!
```

```
openmc.run()
```

```
#####
```

```
#Tally Data Processing
```

```
# Load the statepoint file
```

```
sp = openmc.StatePoint('statepoint.30.h5')
```

```
tally = sp.get_tally(scores=['flux'])
```

```
flux = tally.get_slice(scores=['flux'])
```

```
flux.std_dev.shape = (500, 500)
```

```
flux.mean.shape = (500, 500)
```

```
plt.imshow(flux.mean, interpolation='nearest', cmap='jet')
```

```
plt.title('Flux distribution')
```

```
plt.xlabel('x [cm]')
```

```
plt.ylabel('y [cm]')
```

```
plt.colorbar()
```

```
plt.show()
```

```
tbrplot_tally = sp.get_tally(name='TBR all values')
```

```
tbrplot_tally.std_dev.shape = (500, 500)
```

```
tbrplot_tally.mean.shape = (500, 500)
```

```
plt.imshow(tbrplot_tally.mean, interpolation='nearest', cmap='inferno')
```

```
plt.title('Tritium generation mean result')
```

```
plt.xlabel('x [cm]')
```

```
plt.ylabel('y [cm]')
```

```
plt.colorbar()
```

```
plt.show()
```

```
plt.imshow(tbrplot_tally.std_dev, interpolation='nearest', cmap='inferno')
```

```
plt.title('Tritium generation standard deviation')
```

```
plt.xlabel('x [cm]')
```

```
plt.ylabel('y [cm]')
```

```
plt.colorbar()
```

```
plt.show()
```

```
tbr_tally = sp.get_tally(name='TBR')
```

```
tbr_result = tbr_tally.get_pandas_dataframe()
```

```
yy = tbr_result['mean']
```

```
tbr_total = round(yy.sum(), 3)
```

```
zz = tbr_result['std. dev.']
```

```
error = round(zz.sum(), 4)
```

```
print('*****')
```

```
print('*****')
```

```
print('TBR PRODUCTION IN FLiBe')
```

```
print(tbr_result)
```

```
print('*****')
```

```
print('*****')
```

```
print('TBR total IN FLiBe')
```

```
print(tbr_total, '+/-' , error)
```

```
#Source plotting 2D and 3D
```

```
plot_tokamak_source_3D(my_plasma, "neutron_source_density")
```

```
plt.title('Neutron source density 3D')
```

```
plt.show()
```

```
scatter_tokamak_source(my_plasma, "neutron_source_density")
```

```
plt.colorbar(label='Neutron source density [neutrons/s/m3]')
```

```
plt.show()
```

```
scatter_tokamak_source(my_plasma, "ion_temperature")
```

```
plt.colorbar(label='Ion temperature [keV]')
```

```
plt.show()
```

```
#####
```

```
#Geometry & Source plotting 2D
```

```
scatter_tokamak_source(my_plasma, "ion_temperature")
```

```
plt.colorbar(label='Ion temperature [keV]')
```

```
root_universe.plot(width=(1000, 1000), basis='xz', alpha=0.5,
```

```
                    colors={plasma: 'white', first_wall: 'red',
```

```
                    'lightslategrey', channel: 'aqua',
```

```
                    'aqua', str2: 'lightslategrey',
```

```
                    str1:
```

```
                    nmult:
```

```
                    blanket: 'aqua'})
```

```
plt.title('Source inside geometry')
```

```
plt.show()
```

```
# Plot neutron spectra on STR1
```

```
spectrastr1_tally = sp.get_tally(name='structural_layer_spectra_STR1') # add another tally
```

```
spectrastr1_tally_result = [entry[0][0] for entry in spectrastr1_tally.mean]
```

```
spectrastr1_tally_std_dev = [entry[0][0] for entry in spectrastr1_tally.std_dev]
```

```
spectrumstr1 = []
```

```
spectrumstr1.append(0)
```

```
spectrumstr1.extend(spectrastr1_tally_result)
```

```
plt.loglog(energy_bins, spectrumstr1, linewidth=1)
```

```
plt.xlabel('Energy eV')
```

```
plt.ylabel('Neutrons per cm2 per source neutron')
```

```
plt.title('Neutron spectra STR1')
```

```
plt.grid(True, which="both", ls="--", color='0.65')
```

```
plt.show()
```

```

traces=[]
traces.append(Scatter(x=energy_bins,
                    y=spectrastr1_tally_result,
                    name='breeder_blanket_spectra_STR1',
                    line=dict(shape='hv')
                    )
            )

layout = {'title':'Neutron spectra STR1',
        'hovermode':'closest',
        'xaxis':{'title':'Energy eV',
                'type':'log'},
        'yaxis':{'title':'Neutrons per cm2 per source neutron',
                'type':'log'},
        }

plot({'data':traces,
     'layout':layout
     },
     filename='STR1_spectra.html'
     )

```

# Plot neutron spectra on STR2

```

spectrastr2_tally = sp.get_tally(name='structural_layer_spectra_STR2') # add another tally
spectrastr2_tally_result = [entry[0][0] for entry in spectrastr2_tally.mean]
spectrastr2_tally_std_dev = [entry[0][0] for entry in spectrastr2_tally.std_dev]

spectrumstr2 = []
spectrumstr2.append(0)

```

```
spectrumstr2.extend(spectrastr2_tally_result)

plt.loglog(energy_bins, spectrumstr2, linewidth=1)
plt.xlabel('Energy eV')
plt.ylabel('Neutrons per cm per source neutron')
plt.title('Neutron spectra STR2')
plt.grid(True, which="both", ls="--", color='0.65')
plt.show()
```

# Appendix B

Example of inventory input file for FISPACT-II.

CLOBBER

JSON

GETXS 0

GETDECAY 0

FISPACT

\* FNS 1 year alloy A

DENSITY 12.36

MASS 1.0E-3 5

V 30.00

CR 10.00

W 40.00

TA 10.00

TI 10.00

MIND 1E3

GRAPH 3 2 1

3 1 2

UNCERTAINTY 2

HALF

HAZARDS

<< -----irradiation phase----- >>

FLUX 7.54E+14

ATOMS

TIME 1.0 YEARS

ATOMS

<< -----cooling phase----- >>

FLUX 0.

ZERO

TIME 1 SECS ATOMS

TIME 4 SECS ATOMS

TIME 25 SECS ATOMS

TIME 30 SECS ATOMS

TIME 1 MINS ATOMS



TIME 50 YEARS ATOMS

TIME 50 YEARS ATOMS

END

\* END

/\*

## **Ringraziamenti**

In conclusione di questo lavoro desidero ringraziare, nella mia lingua madre, tutti coloro che hanno contribuito in modo diretto o indiretto al conseguimento di questo traguardo. Il professor Zucchetti e la professoressa Testoni che hanno reso possibile la stesura di questa tesi ed i dottori Segantin e Meschini per le loro correzioni e la pazienza che hanno dimostrato. I miei genitori, che mi hanno sostenuto materialmente ed incoraggiato emotivamente in tutti questi anni; mio fratello, che ha rinunciato alla mia compagnia in molte serate devolute allo studio; le mie nonne, che mi hanno accompagnato con affetto ed i miei nonni, che purtroppo non sono riusciti a vedere il frutto di tante fatiche. La mia compagna Tereza, che con pazienza ha ascoltato per mesi i miei continui cambi di opinione ed i miei vaniloqui su argomenti che probabilmente le interessavano molto meno di quanto non desse a vedere; mia cugina Martina, il cui aiuto è stato fondamentale per supplire al mio pessimo inglese; le mie amiche di una vita Mara e Claudia, con i loro utili consigli. Un ringraziamento speciale va al mio caro amico Davide Pettinari: la sua collaborazione è stata fondamentale e la sua amicizia il risultato più bello di questo percorso.